2016

FINITE ELEMENT ANALYSIS AND TOPOLOGY OPTIMIZATION OF DIFFERENTIAL CASE AND CONTROL ARM FOR STATIC AND FATIGUE LOADING

Pankaj N. Kalan
Michigan Technological University, pnkalan@mtu.edu

FINITE ELEMENT ANALYSIS AND TOPOLOGY OPTIMIZATION OF DIFFERENTIAL CASE AND CONTROL ARM FOR STATIC AND FATIGUE LOADING

By

Pankaj N. Kalan

A REPORT

Submitted in partial fulfillment of the requirements for the degree of

MASTER OF SCIENCE

In Mechanical Engineering

MICHIGAN TECHNOLOGICAL UNIVERSITY

2016

This report has been approved in partial fulfillment of the requirements for the Degree of MASTER OF SCIENCE in Mechanical Engineering.

Department of Mechanical Engineering-Engineering Mechanics

Report Advisor:	*Dr. Gregory Odegard*
Committee Member:	*Dr. Paul Sanders*
Committee Member:	*Dr. Paul J. van Susante*
Department Chair:	*Dr. William Predebon*

Table of Contents

List of Figures

List of Tables

Acknowledgements

I would like to thank my advisor Dr. Gregory Odegard for his continuous support and encouragement which helped me complete this research. His technical expertise and calm approach towards solving my problems helped me not only in becoming a better engineer but a better human being. I would also like to thank Dr. Paul G. Sanders for helping me apply the concepts of Material Science towards my research. In addition, I would like to thank Dr. Paul van Susante for his valuable feedback.

I feel myself fortunate to work with Mr. Russell Stein, Mr. Parag Deshpande, Ms. Stephanie Tankersley, Ms. Alejandra Almanza Perales and Mr. Swapnil Pandey, who helped me during my research at every step.

I would also like to thank fellow graduate students Mr. Prasad Soman and Ms. Amruta Kulkarni for their help. Special thanks to all my friends in Houghton for their support.

Finally, I would like to thank my family, without whom this could not have been possible.

Abstract

Optimization of the automobile components can result in a significant decrease in vehicle weight, increase in fuel efficiency and reduction in environmental damage. For example, the lightweight vehicle production will save over 4.4×10^9 GJ of energy and 4.1×10^8 tons of CO2 over a 10 year period, compared to the current non-light weight vehicles. This equates to 890 billion miles or 42 billion gallons of gas savings (Wu 2016). This study evaluates the weight reduction possible by using manual and automatic (using Optistruct software) topology optimization processes. Optimization of a vehicle differential case done in this study shows that a weight reduction of up to 38% is possible without affecting the safety of the component. The manual optimization methodology used for this process can be implemented for any other cast component. In addition to this, a comparative study is performed of topology optimization (using Optistruct software) on a control arm considering static loading conditions and fatigue (dynamic) loading conditions. Comparison of those optimization results shows that the resulting component of the topology optimization having a constraint for fatigue life performs better in fatigue loading analysis. The majority of the research papers related to topology optimization consider only static loads during the optimization setup and then the resultant optimized component is analyzed for fatigue safety. But instead of this approach, the consideration of an additional fatigue constrains in the optimization problem formulation may give a resultant component with comparatively better life under fatigue loading. This assumption is proved to be right from the results of the study performed on the control arm.

1. Introduction

Why topology optimization of automobile components?

The automobile industry is in a continuous struggle to reduce the weight of the cars for multiple reasons. It helps to increase the fuel efficiency and thereby reduces the emissions. The reduction in weight is caused by reducing the size or number of parts which reduces the manufacturing costs. Even the growth of emerging electric vehicles is dependent on better mileage per charge which is achievable by, among other methods, through weight reduction.

This weight reduction can be achieved mainly by two methods. The first one is using alternatives to the traditionally used materials such as steel and ductile iron. For example, the increase in use of aluminum to replace steel in manufacturing structural elements in vehicles (Cole and Sherman 1995). But there are major hurdles involved such as the high cost of manufacturing (Kelkar, Roth et al. 2001) due to which it is used mostly in luxury vehicles. The use of lighter materials may even lead to negative environmental impact when their entire life cycle is considered due to their production and manufacturing processes and limitations in recycling (Witik, Payet et al. 2011).

The other method, which has been implemented in this study is reducing the weight of the component by using topology optimization (Uwe Schramm 2006). This method is comparatively easier to implement than the previous one as there is less cost of transition involved. We can redesign a structural component without changing its assembly or its manufacturing process. Hence it can be easily implemented in low end vehicles as well without affecting the prices.

Scope of this project:

LIFT (Lightweight Innovations for Tomorrow) is a collaboration between industry and academic partners and operated by American Lightweight Materials Manufacturing Innovation Institute. It is working towards developing manufacturing technologies for implementing lightweight materials. This is their first project on the use of iron alloys for thin-wall casting of differential case and is funded and controlled by them. This report is a part of that project and covers the mechanical design aspects of the differential case. The remaining part about developing an alloy that can allow manufacturing of this part with thin-wall casting was done by material science and technology team at Michigan Tech. Manual topology optimization of the differential case reduced its weight by nearly 38%.

The second part of the project is to design a part in fatigue loading. But the actual selection of part is not yet done by LIFT. Hence, an automobile control arm was selected for fatigue optimization. Optistruct was used to perform the topology optimization. Two analysis were performed considering the static loading condition and the fatigue loading condition, respectively. Different results were obtained from these processes, which were compared for fatigue loading life. The later one was showed to be having better strength for fatigue loading.

2. Part details

This section includes the details of the two parts, the differential case and the control arm, which have been optimized for weight reduction.

2.1 Differential case:

The manual optimization of this part was previously done by Mr. Parag Deshpande (Deshpande 2016). This report is in continuation to his work to get better optimization results with lower stress values (below the yield limit of the material) to ensure safety of the component. The data used for this part (part geometry, loading and material data) has been provided by Eaton.

2.1.1 Part function:

Differential gear box is an assembly with three shafts which may act as input or output (at any time, there must be at least one input and one output shaft for its functioning). In automobiles, one shaft serves as input (which is connected to the engine) and the other two work as output (which are connected to the driving wheels). The gear mechanism inside the casing distributes the shaft speeds such that rotation speed of the input shaft is the average of the rotation speed of the two output shafts while maintain a constant torque ratio. This balances the increase in speed of one wheel by reducing the speed of the other wheel. And helps in maneuvers which require different speeds for each wheel such as cornering.

Figure 1 and Figure 2 shows differential assembly which consists of outer casing and internal gear mechanism that transfers the torque from the transmission shaft to wheel axles.

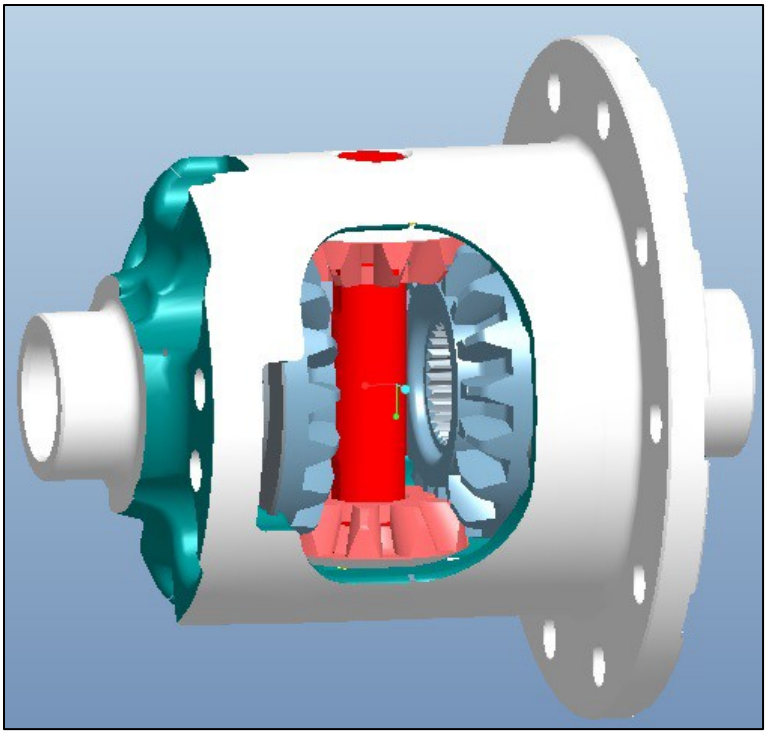

Figure 1. Differential case assembly (Klipfel 2016)

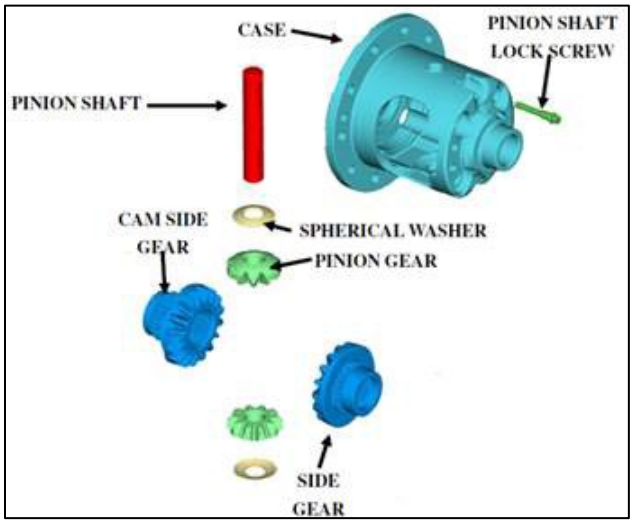

Figure 2. Exploded view of differential case (Klipfel 2016)

The ring gear is connected to the differential case and transfers the torque from transmission shaft (attached to the bevel gear) to the differential case as shown in Figure 3.

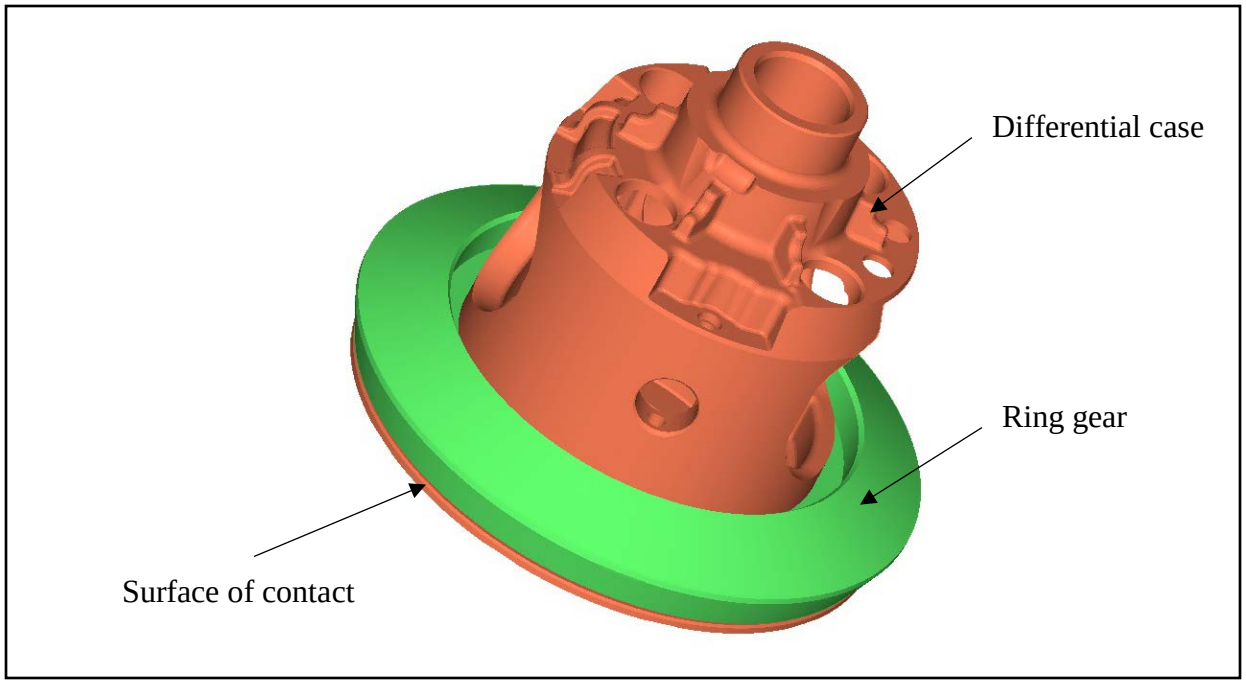

Figure 3. Assembly of differential case with ring gear

For this report, we will be considering only the differential case for optimization to reduce its weight.

2.1.2 Loads and boundary conditions:

Specific terminologies are used to denote different areas of the differential case to enable ease of understanding. These terms are shown in Figure 4.

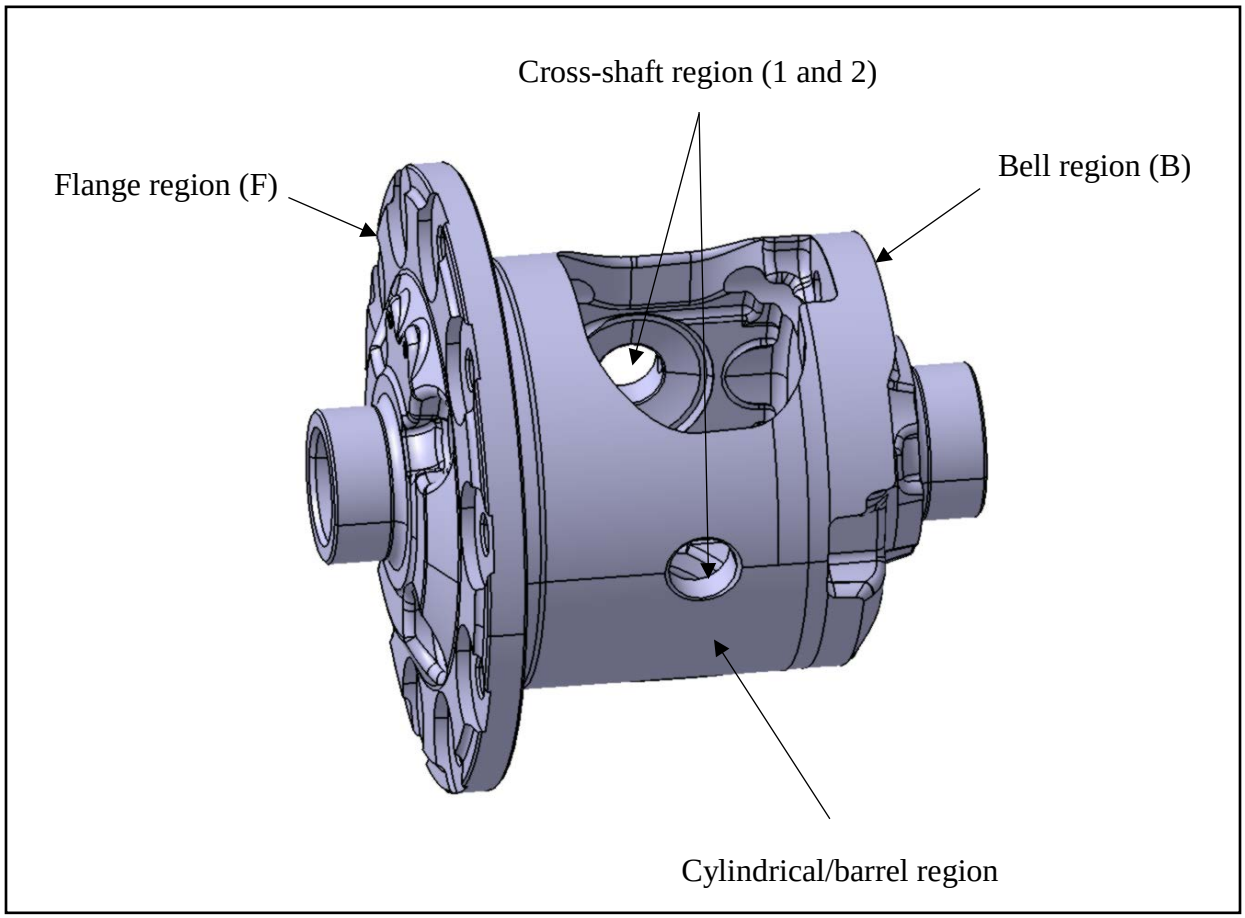

Figure 4. Differential case terminology

The flange is attached to the ring gear, the cylindrical region houses the gear assembly and the cross –shaft region supports the pinion shaft.

The magnitude of the forces acting on the differential case is given in Table 1 and their location is shown in the free body diagram in Figure 5.

Table 1. Differential case external load data (provided by Eaton)

	Load	Force magnitude (N)	Surface area (mm2)		Pressure
1	Pinion gear force	15381.18	948.68	1	16.21
			948.68	2	16.21
2	Side gear force	26150.90	907.90	F	28.8
			2460.52	B	10.63
3	Bearing preload	2224.00	875.66	F	2.54
			902.00	B	2.47
4	Cross shaft load	51883.22	187.93	1	276.08
			187.92	2	276.09
5	Ring gear radial force FORWARD	34140.2	NA		NA
6	Ring gear axial force FORWARD	7589.4	NA		NA
7	Ring gear radial force REVERSE	34140.2	NA		NA
6	Ring gear axial force REVERSE	7589.4	NA		NA

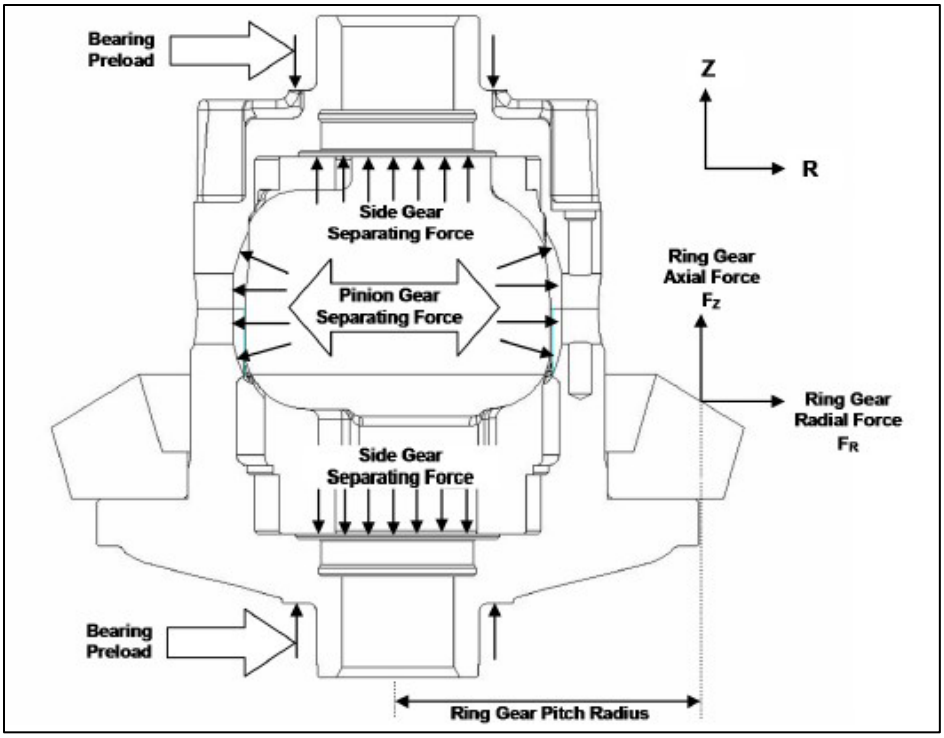

Figure 5. External forces on differential case

The differential case is free to rotate along its axis but its translational motion is constrained in x, y and z direction at the flange end and x and y direction at the bell end. The ring gear has 36 teeth. The forces act on each of these teeth sequentially and hence are considered as 36 different static load steps for FEA as shown in Figure 6.

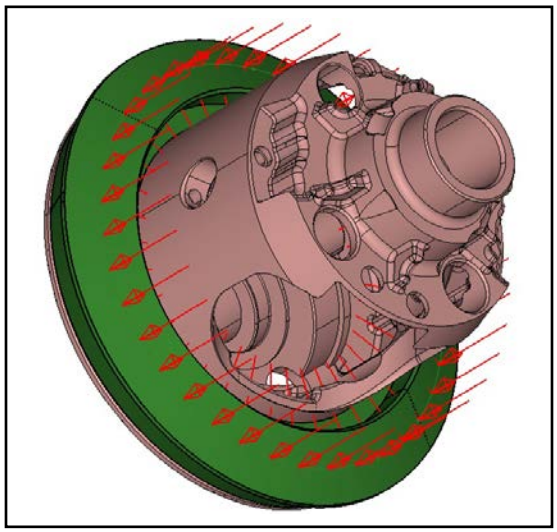

Figure 6. Forces at each tooth on the ring gear

2.1.3 Material:

The material used for differential case is D7003 (Ductile Iron Grade D7003), which is currently used for manufacturing the differential case. Its properties are shown below in Table 2 and Table 3.

Table 2. Material properties for differential case (provided by Eaton)

Young's modulus	1.72e5 MPa
Poisson's ratio	0.275
Yield strength	490 MPa Min
Ultimate tensile strength	773 MPa Min

The material used for ring gear is steel with following properties (provided by Eaton):

Table 3. Material properties for ring gear (provided by Eaton)

Young's modulus	2.07e+05 MPa
Poisson's ratio	0.3

2.2 Control arm:

The second part of the LIFT project had not been decided when this study was done, but it was supposed to be a fatigue component. Hence, the topology optimization was performed on the control arm for fatigue loading. The data used for this analysis was taken from Altair website.(2016)

2.2.1 Part function:

Control arm (also called as A-arm due to its shape) is a hinged component connecting the chassis to the suspension system/wheel hub. It has two mountings attached to the chassis forming a hinge and the third end is attached to the wheel knuckle. It also serves as a mounting point for the suspension system. This enables the motion of the wheel in vertical direction which is controlled by the suspension system.

2.2.2 Loads and boundary conditions:

The forces acting on a control arm can be separated into four types as per their cause (Song, Park et al. 2009). First one is the static total weight of the vehicle, which results in static loading conditions. Others include the loads due to braking and cornering conditions respectively and the loads due to bumping of the vehicle caused by the road conditions. Those last three forces are time dependent and cause fatigue loading.

The cylindrical surfaces at the end of two arm are hinged at the chassis along their axis (taken as x axis in model) but are free to move in translational motion along the axis. Hence, one of them is constrained for translational motion along y and z axis and the other one is constrained for translational motion along z axis. The rotation of the control arm along this axis is prevented by a third constrained applied at the central hole for translational motion

along all three axes. The static loads are acting on the two ends hinged to the chassis while the fatigue loads are acting on the end attached to the wheel. The resultant forces acting on the control arm are shown in Figure 7.

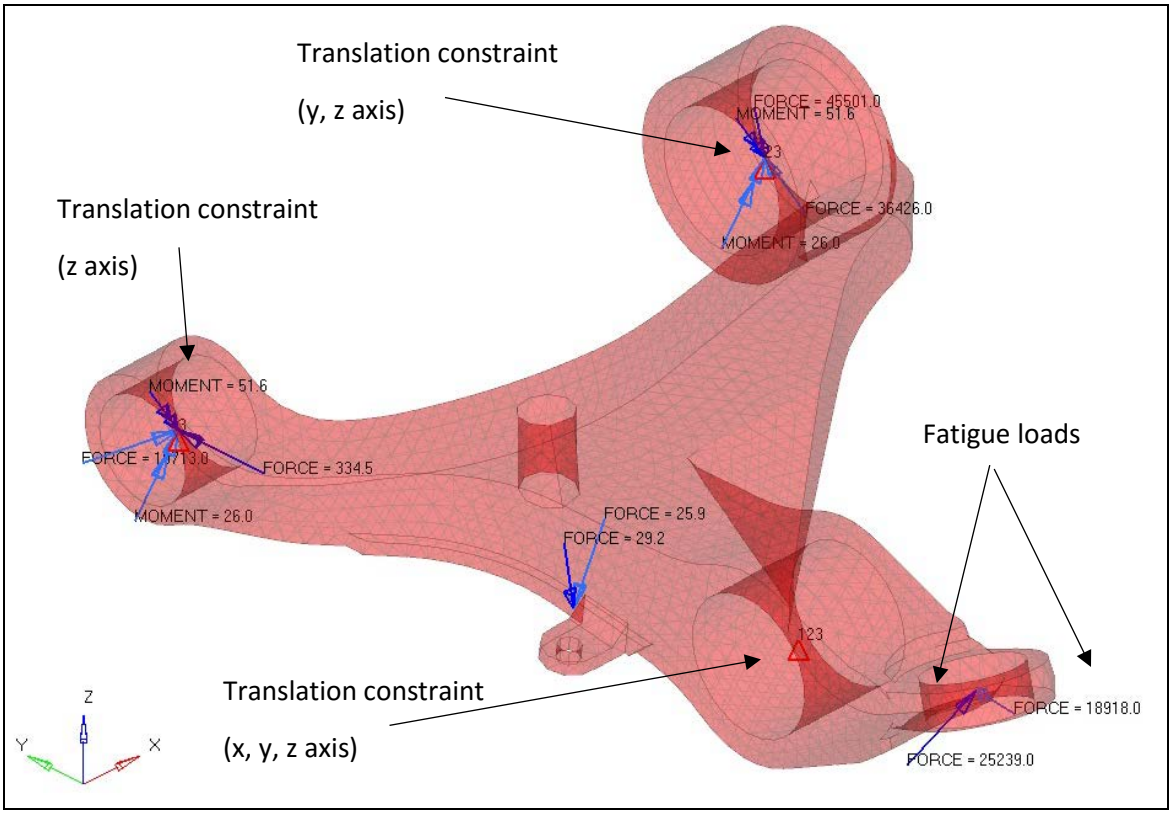

Figure 7. External loads and constraints on control arm

The loading data for the variable loads used for the analysis (taken from Altair website) is plotted as load amplitude factor (y axis) against time (x axis) for a time period of 2545 seconds with a frequency of 1 Hz. The data is shown in Figure 8 and Figure 9.

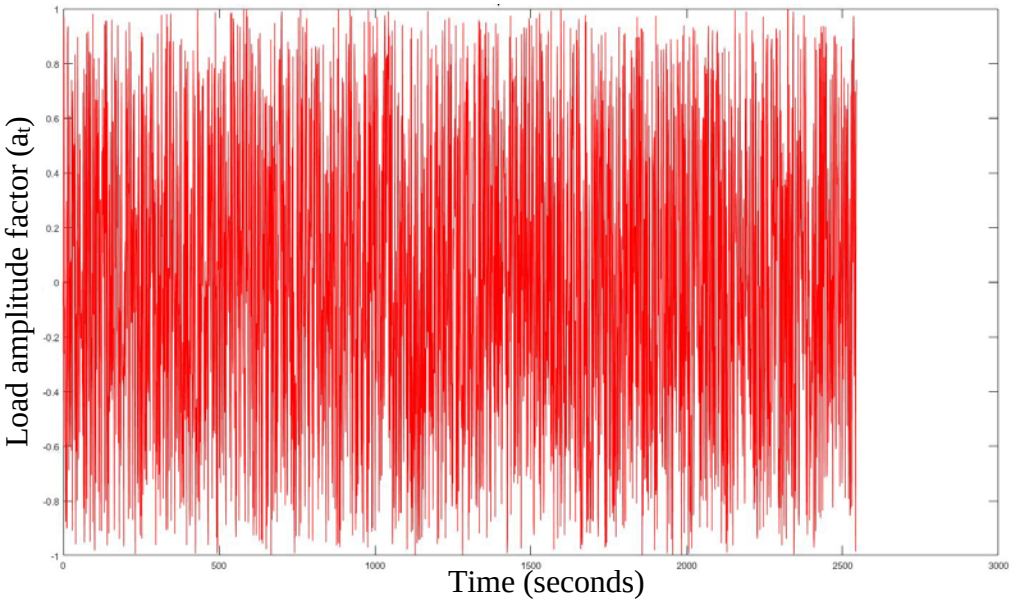

Figure 8. Load amplitude factor vs time for load 1

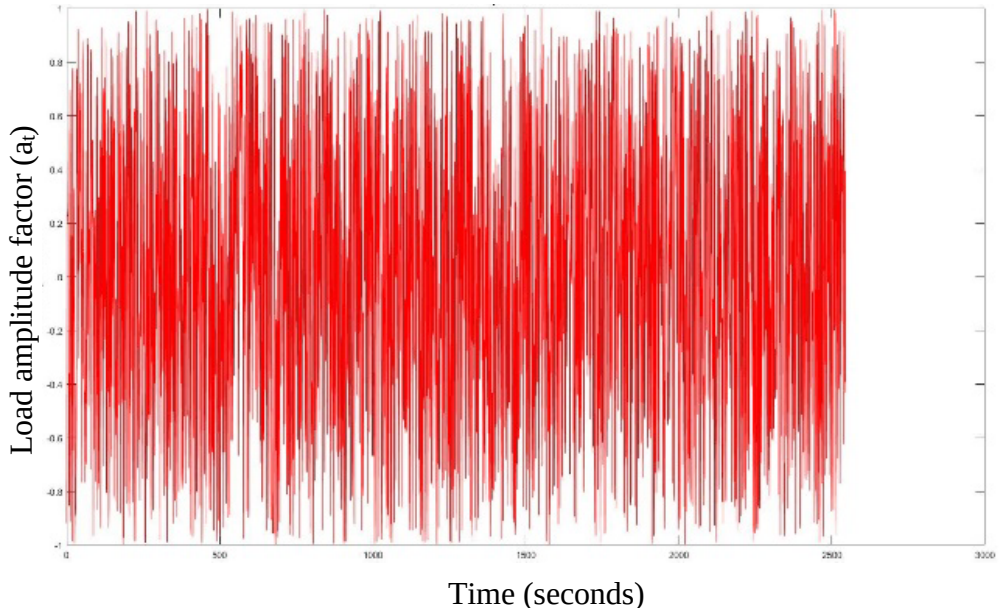

Figure 9. Load amplitude factor vs time for load 2

The instantaneous force acting at any time is given by,

f_t (instantaneous force at given time t) = F (magnitude of the load applied) * a_t (load amplitude factor at that time)

Where, the load amplitude factor varies from +1 to -1 and instantaneous force ft varies from +F to –F, respectively.

2.2.3 Material:

The material used for this part is Grade 900 ADI (austempered ductile iron) with following properties as shown in Table 4.

Table 4. Material properties for control arm (taken from Applied Process website):

Static properties	
Tensile strength	900 MPa
0.2% offset yield strength	650 MPa
Elongation (% in 2inch gage length)	9
Hardness Brinell BHN (B.I.D. mm)	302 (3.50)
Young's modulus	159.3 GPa
Compressive strength	1380 MPa
Shear strength	870 MPa
Modulus of rigidity	65.1 GPa
Poisson's ratio	0.25
Dynamic properties	
Strength coefficient K	1503 MPa
Strain hardening exponent n	0.143
True fracture strength sf	1032

True fracture ductility ef	0.082
Strength coefficient K'	1538 MPa
Strain hardening exponent n'	0.133
Fatigue strength coefficient sf'	1455 MPa
Fatigue strength exponent b	-0.111
Fatigue ductility coefficient ef'	0.199
Fatigue ductility exponent C	-0.677

3 FEA analysis setup:

3.1 Differential case:

3.1.1 Geometry:

The part data was received from Eaton. The ring gear was larger in size and was scaled down to match the size of differential case. The geometry of the differential case and the ring gear was assembled in CATIA and converted into IGES file so that it could be imported in Hypermesh. The geometry was cleaned using the 'autoclean' tool in Hypermesh (Geom>autoclean) with 'target element size parameter' set to 1. It removes features smaller than the target element size and closes small gaps between edges and creates a closed surface.

3.1.2 Meshing:

The differential case is meshed using 2D tria elements to enable easier element quality control. It is generated using the 'automesh' function (2D > automesh) to get the 2D mesh from the surfaces. The 'QI optimize' option was used which optimizes the mesh generated as per the element size (taken as 1 mm), mesh type (selected as tria) and feature angle (set to 30) and default criteria for other element properties. First order connectivity was used to generate elements from the surfaces. Parag had considered the element size of 2mm for his analysis. This element size was further reduced to 1 mm, which was required to get better mesh quality at the small features (minimum thickness of nearly 2.5 mm) present in the optimized differential case as per the mesh validation using von Mises stress convergence criteria. The mesh details are shown in Figure 10.

This mesh is then used to generate 3D tetra elements in the solid (3D > tetramesh). The tetramesh option was used and the already created 2D mesh was selected for the 'Fixed

trias/quads to tetra mesh' option. The quality of the tetra mesh was later improved using the 'tetra mesh optimization' tool in utility tab (Utility > Geom/Mesh > Tetra Mesh Optimization) with the minimum tet collapse value set to 0.1 and other values set to default. The 3D mesh for the ring gear was created by following similar procedure as before. The ring gear mesh was connected with the differential case to transfer the forces acting on the ring gear to the differential case. 1D CWELD elements were used for this purpose (1D > spotweld). This required extraction of 2D mesh from the 3D mesh at the contact surface between differential case and ring gear. These 2D elements were later used to generate the 1D connecting elements.

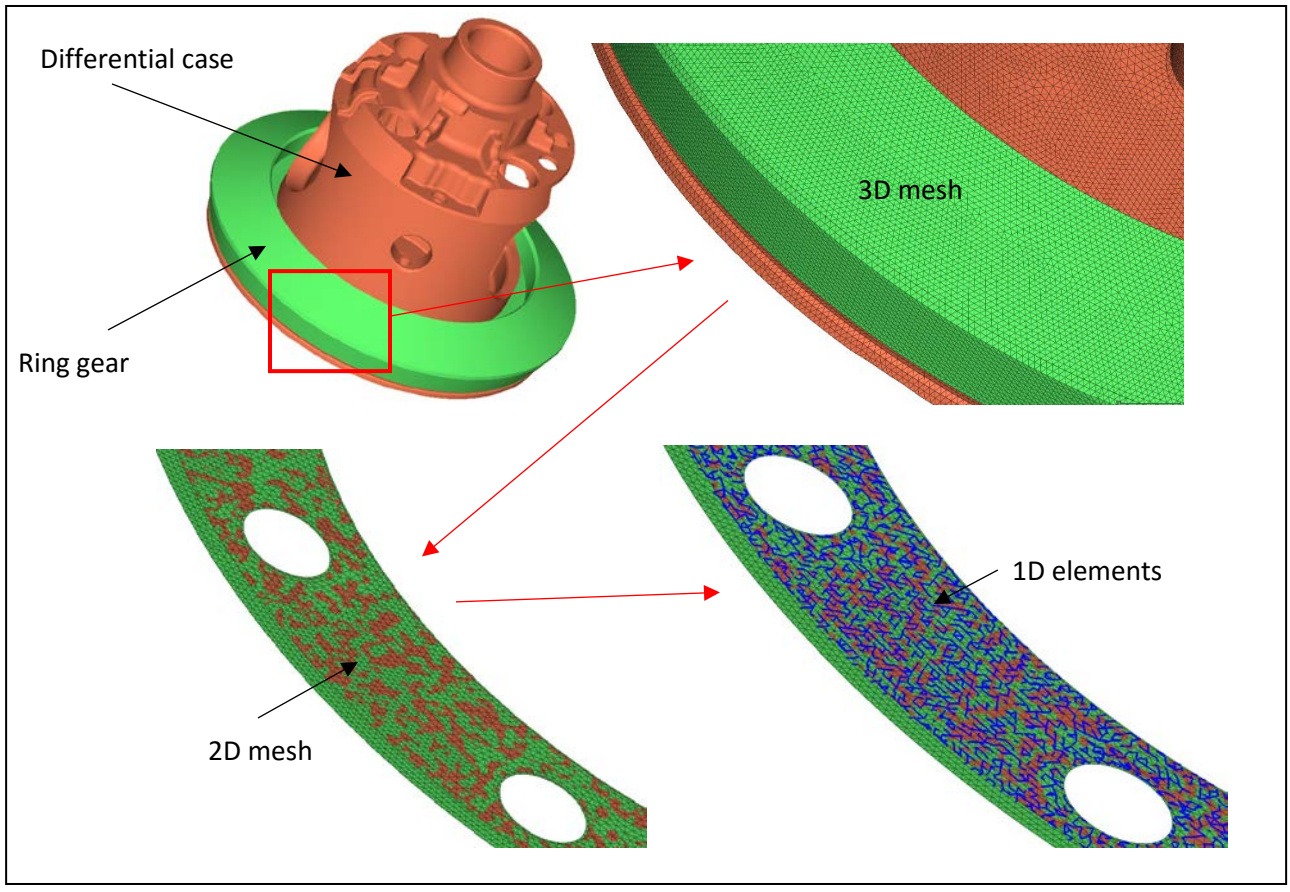

Figure 10. 2D elements (in green and orange) extracted from 3D elements to create 1D connecting element (blue)

3.1.3 External loads and boundary conditions:

Hypermesh uses modules called ‘Load Collectors’ to store the loads and ‘Load Step’ to store a loading condition. Load collectors are linked to load step to define a loading condition. Multiple load collectors were created to accommodate all the types of loading conditions on the differential case. One load collector has all the pressures acting on the differential case due to other components in contact except the ring gear (the details have been included in previous section) created by using the ‘pressures’ function (Analysis > pressures). The second load collector includes all the constraints added by using ‘constraints’ function (Analysis > constraints). This includes the translational constraints applied to the mounting surfaces (inner side of the cylinders at the bell and flange end) which have been explained previously. As per our consideration to analyze the forces on each tooth separately, we have created 36 different load collectors to include the forces at each tooth. These forces are distributed on the outer surface of the ring gear separated by 10 degrees (360 degrees divided by 36 teeth) along the axis. Also, the pressure load collector needs ‘LOAD’ card image which cannot include the ring gear forces acting at a single point. Hence, separate 36 load collectors were used to combine the pressure load collector with each of the ring gear force load collector. These were then linked along with the constraint load collector to create 36 load steps. This setup can be shown as below:

(Pressure load collector) + (n^{th} ring gear force load collector) = (n^{th} combined load collector)

and

(n^{th} combined load collector) + (Constraints load collector) = (n^{th} load step),

where n=1 to 36.

3.2 Control arm:

3.2.1 Geometry:

The geometry of the control arm was cleaned by following the same process which was used for the differential case.

3.2.2 Meshing:

The 2D and 3D mesh was created following the same method as the differential case. A rough 2D mesh was created for this part. As this is a comparative study between static and fatigue optimization, the absolute values of the von Mises stress was less important. Also, the time required for running the optimization increases rapidly with decrease in element size. Hence a large element size of 10mm was used in this case to restrict the analysis time.

3.2.3 External loads and boundary conditions:

The external loads are of two types, static and fatigue; and there are two loading conditions (for both static & one static and one fatigue case). Hence we have four load steps, two each for static and fatigue loads. The load steps(LS) created from the load collectors (LC) are given below:

LC_{1S} (static load 1) + LC_{1F} (fatigue load 1, applied as static) + LC (constraints) = LS_1 (static)

LC_{2S} (static load 2) + LC_{2F} (fatigue load 2, applied as static) + LC (constraints) = LS_2 (static)

LC_{1S} (static load 1) + LC_{1F} (fatigue load 1, varying with time) + LC (constraints) = LS_1 (fatigue)

LC_{2S} (static load 2) + LC_{2F} (fatigue load 2, varying with time) + LC (constraints) = LS_2 (fatigue)

Along with this, an additional setup is required for the fatigue analysis. The flowchart to create this setup in Hypermesh is shown below in Figure 11.

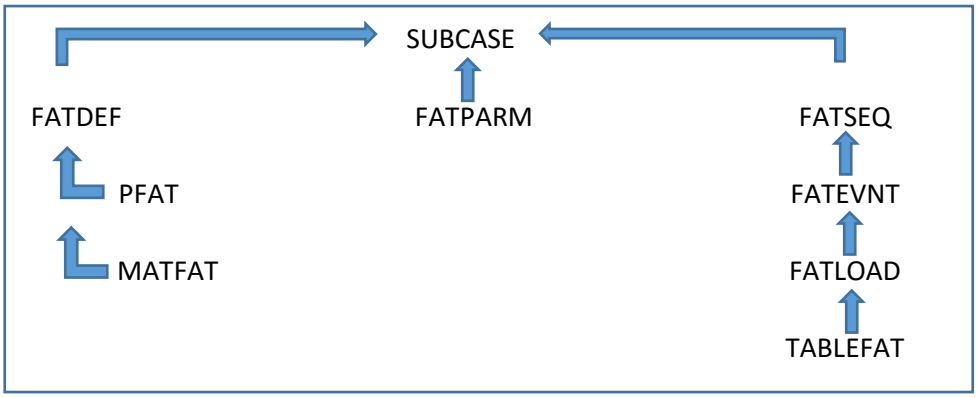

Figure 11. Flowchart of fatigue load setup in Optistruct (Hyperworks Help Manual)

The fatigue SUBCASE is formed of three properties which are again defined by their sub-properties. Their brief details are given below and the screen capture of the same is shown in Figure 12:

MATFAT: This includes the fatigue properties of the material used for analysis. We are using Strain-Life method to predict the fatigue life. Hence, need to select E-N analysis type and add all the material properties mentioned previously in Table 4.

PFAT: This includes the remaining properties of the part such as any treatment or finish given to the part and the fatigue reduction factor of the elements. We don't have any such values for our part.

FATDEF: Combines the previous two material and manufacturing properties.

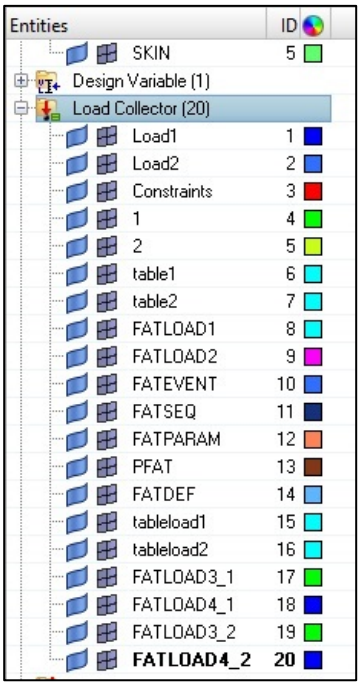

Figure 12. Load collector setup for fatigue load case

FATPARM: This includes the parameters used for the fatigue analysis, i.e. stress combination method, mean stress correction method, rainflow parameters and stress units (MPa was used for control arm analysis).

TABLEFAT: This includes the loading history of the fatigue load added as a table with y axis defining the amplitude of load and x axis defining the time.

FATLOAD: Defines which TABLEFAT, i.e. loading history data has been assigned to which load collector.

FATEVNT: This includes all the FATLOADS, i.e. fatigue loads applied to the model.

FATSEQ: Defines the loading sequence of the fatigue events created by multiple FATEVNT cards.

4 Manual optimization for static loading:

The design of differential case has been optimized for static loading conditions to reduce its weight by 38% by doing manual modifications in its geometry.

4.1 Parametric model creation:

The CAD data received for the differential case was in IGES format with no construction history. This made it difficult to make modifications to the model. Hence, a parametric model is created in CATIA matching the reference IGES model as shown in Figure 13. It is created in such a way that it would be easy to change the dimensions for key features.

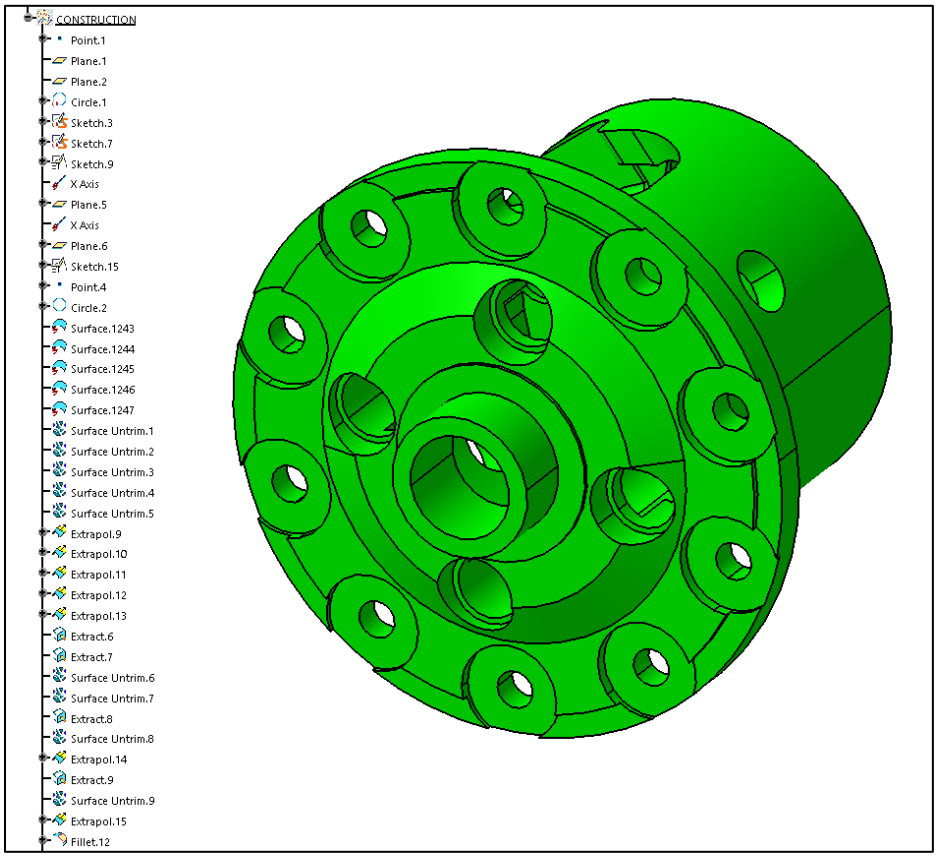

Figure 13. Parametric model of differential case

4.2 Design volume selection:

The model is separated in two volumes as shown previously to enable easy modifications of the design volume without affecting the non-design volume. The total volume of the differential case is divided in two parts as per the part's functional requirements, as shown in Figure 14. This CAD process was completed in CATIA-V5.

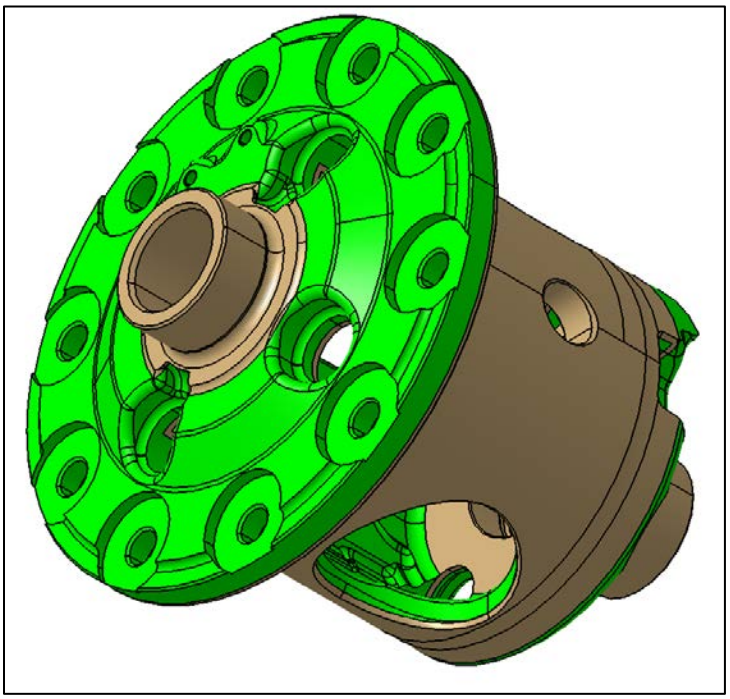

Figure 14. Separation of part into design and non-design volumes

Non-design volume: This volume is required for the assembly of other components on the differential case and cannot be modified. Hence, it is not considered for the optimization process and is left unchanged. It is shown in Figure 15.

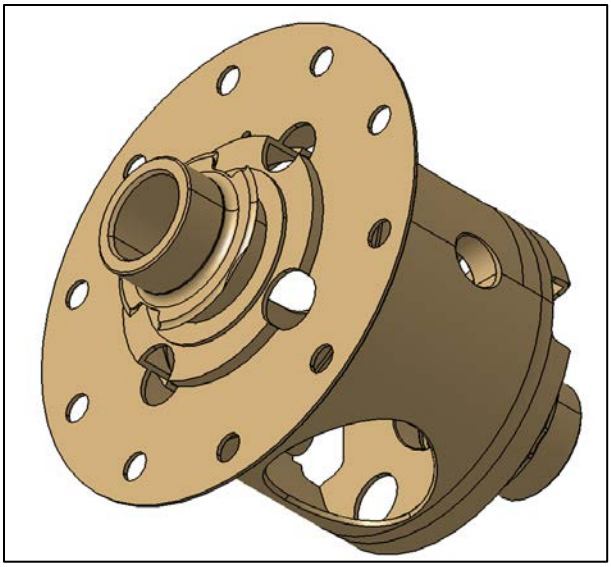

Figure 15. Non-design volume

Design volume: This volume doesn't have any assembly requirements restricting it from any modifications. Although there are some manufacturing restrictions such as cast direction and draft angles that need to be considered while modifying this volume during the optimization process. It is shown in Figure 16.

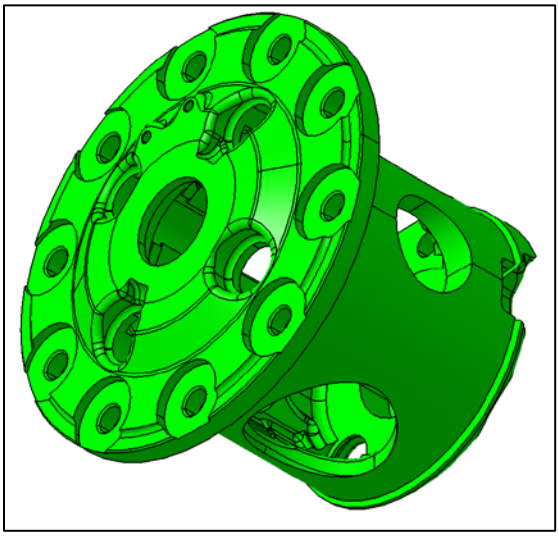

Figure 16. Design volume

4.3 Optimized design:

New optimized models are created by removing material from the baseline model. The areas for material removal are predicted as per the stress distribution of the baseline model. The stresses are found to be very low in the flange region. The new material used for this project is supposed to allow casting thickness as low as 4mm, which could be reduced to 3 mm after machining (This value was taken as per the maximum allowable thickness possible for the material as per the analysis done by MTU Material Science department and mentioned in the report by Alexander D Reinl (Reinl 2016)). There are many areas in the baseline model which have higher part thickness inly for manufacturing feasibility. It can be seen in Figure 17:

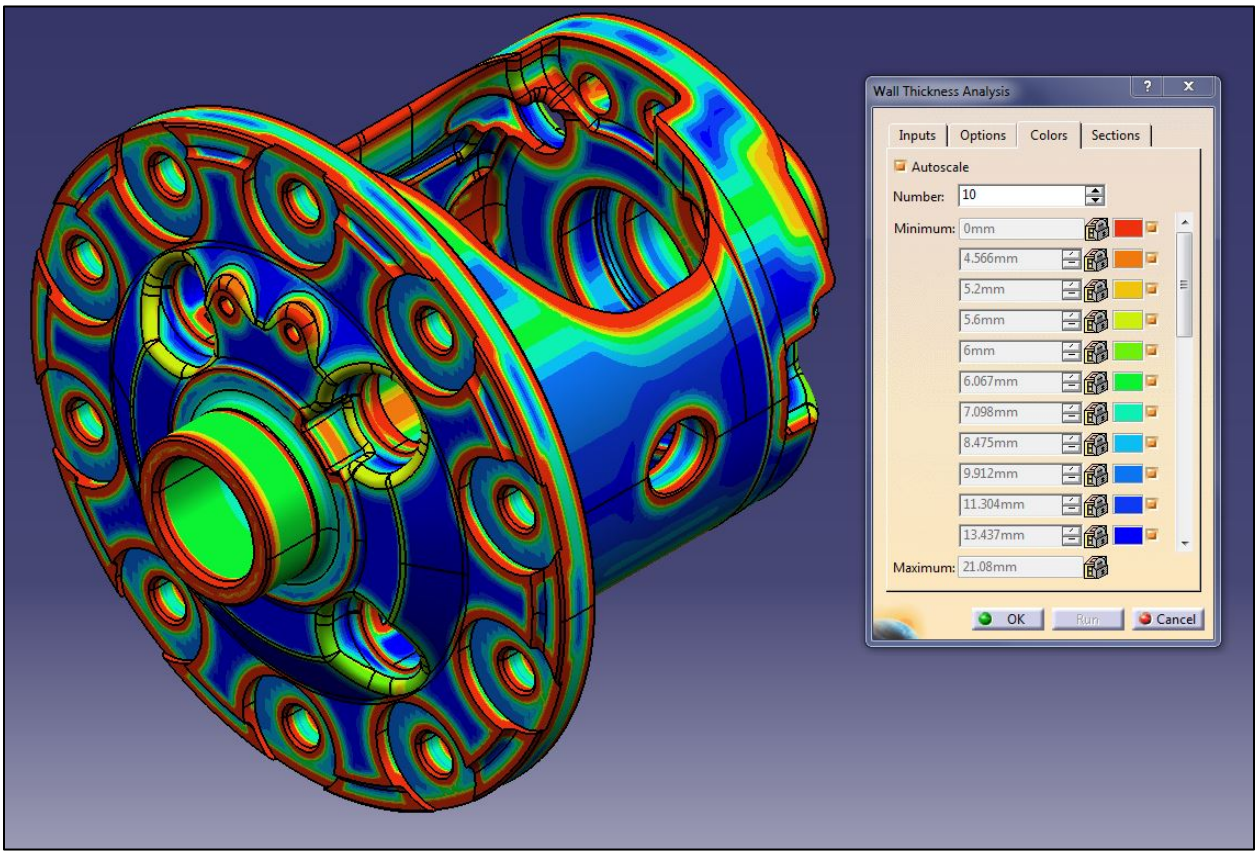

Figure 17. Part thickness analysis

Hence, the flanged is redesigned to a thickness of 3 mm. The area near the bell end has low stress distribution. So the material in this region is removed without affecting the assembly requirements and the part is shown in Figure 18.

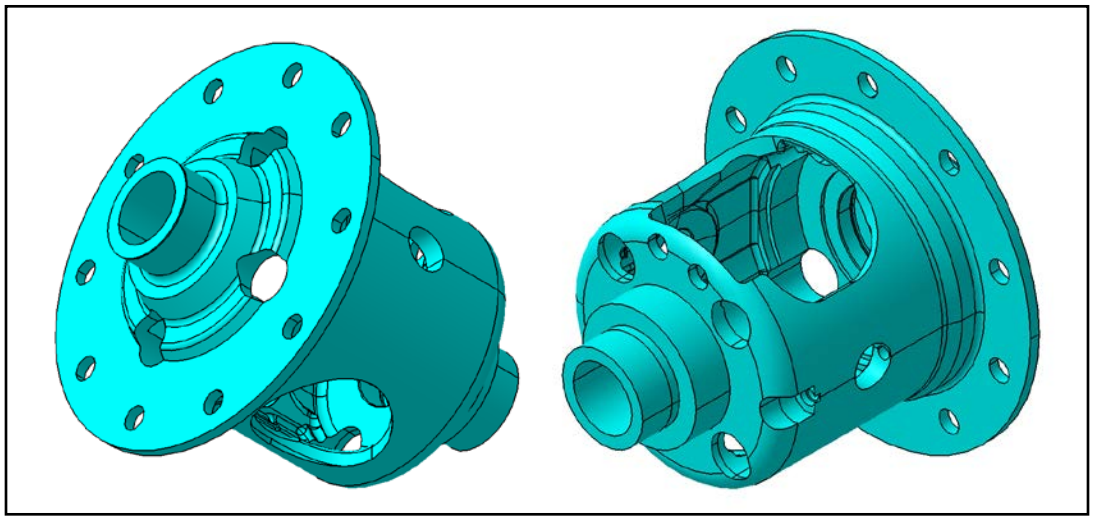

Figure 18. Optimized component designed by me and Mr. Parag Deshpande

Another alternate optimized design is developed by Mr. Jiten Shah, as shown in Figure 19. The major difference between this model and the previous one is the addition of ribs which increases the part strength. This model is used instead of the previous one for further process as per the decision of the LIFT team.

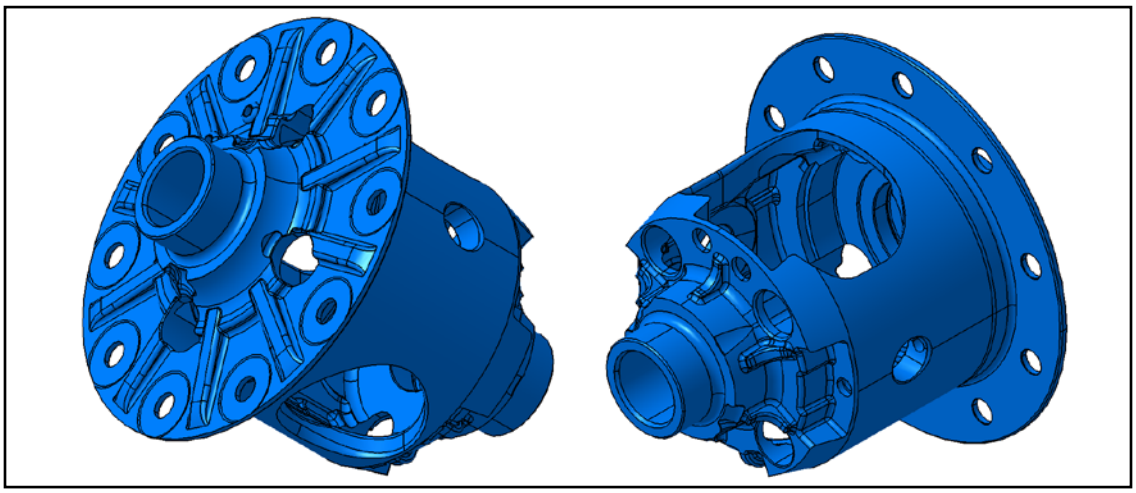

Figure 19. Optimized component designed by Mr. Jiten Shah

4.4 FEA results:

The FEA analysis of the optimized model shows multiple areas of high stress exceeding the yield limit of the material. The areas near the cross shaft region are ignored as per the suggestion from Eaton as the loading in these areas is non-inverting. Other peak stresses are observed in the inner areas of the flange region (as shown in the images below).

The spurious elements occurring in some areas are removed to get a uniform stress distribution. Design iterations were performed to add material in critical areas to reduce the peak stress values. The areas of material addition are as shown in Appendix B.

The resulting reduction in stress is shown in Figure 20, Figure 21 and Figure 22.

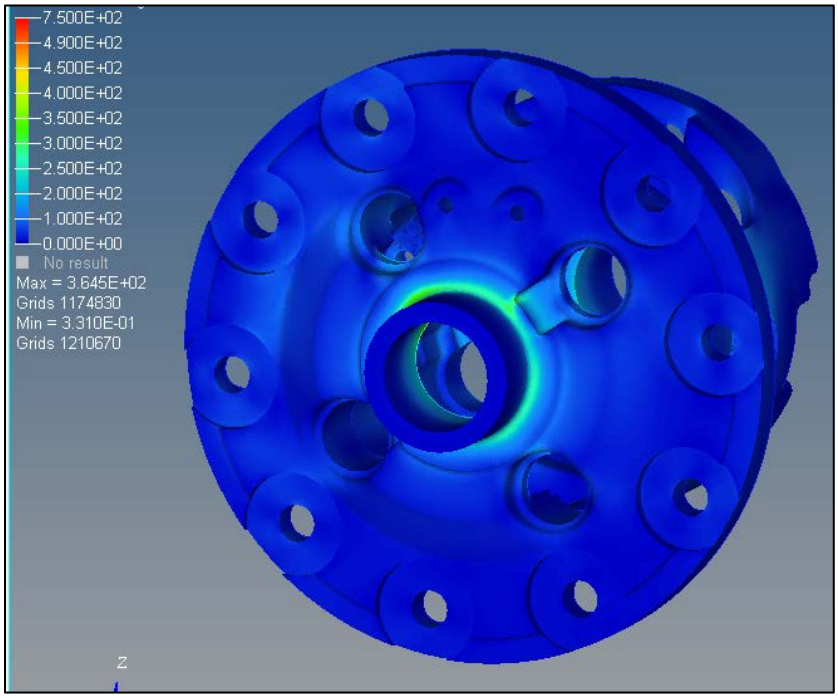

Figure 20. Baseline model von Mises stress distribution

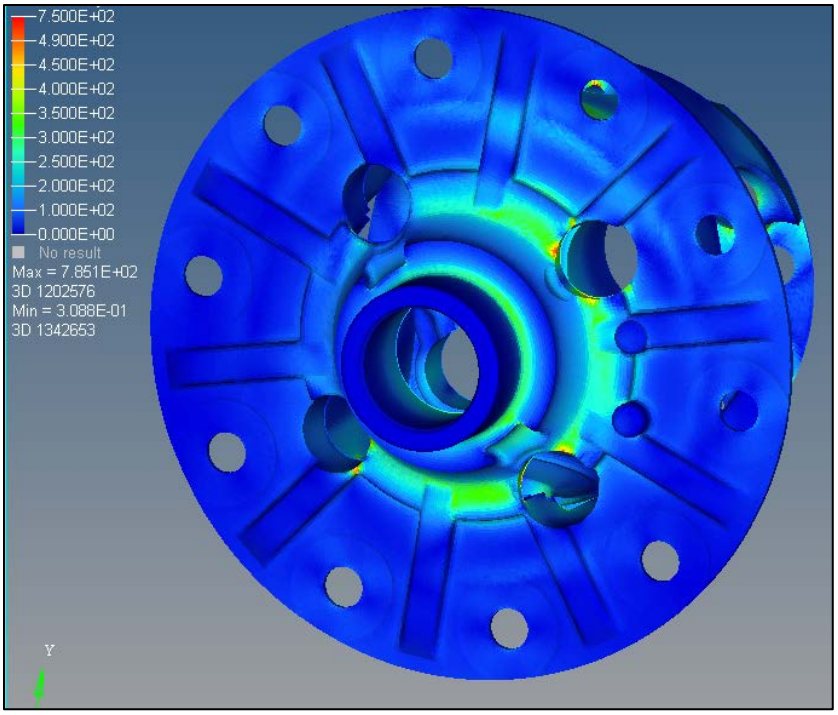

Figure 21. Optimized model von Mises stress distribution

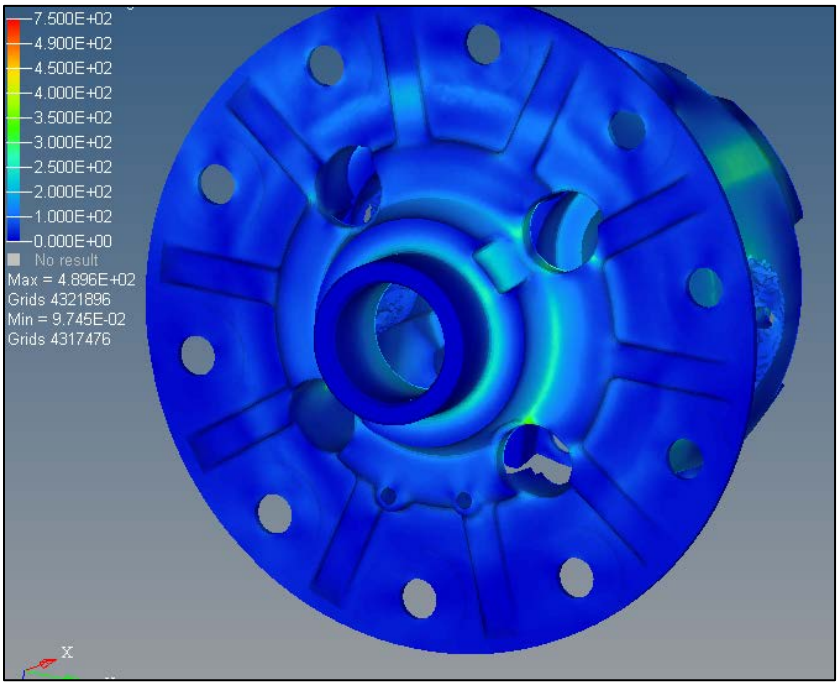

Figure 22. Optimized model with material addition von Mises stress distribution

4.5 Final design:

Final design after all the modifications is as shown below in Figure 23 (the surfaces which need machining after the casting is completed are highlighted in brown color):

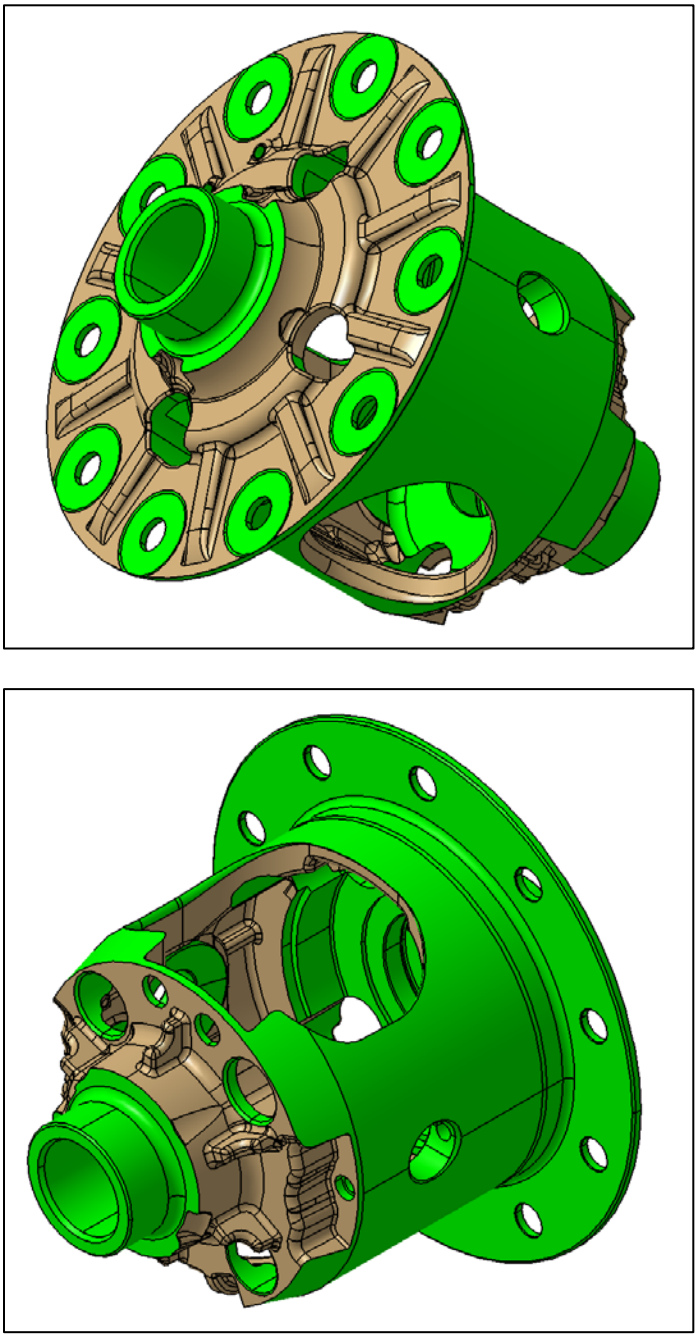

Figure 23. Final optimized design after material addition

Stress comparison between the three models for all the load steps is shown below in Table 5.

Table 5. Stress comparison for baseline, optimized and material added models

	Baseline model	Optimized model	Optimized model with material addition
Average von Mises stress value (MPa)	368.71	828.14	483.86
Volume(m^3)	7.71e-4	4.66e-4	4.82e-4
Mass % w.r.t to baseline	100	60.38	62.5
Mass reduction in % with respect to baseline model	-	39.62	37.5

Hence, we are able to achieve nearly 37.5% reduction in mass due to the manual optimization process.

5 Topology optimization for static loading:

The design of control arm is optimized for static loading conditions by using Optistruct.

5.1 Topology optimization theory:

Mathematically, optimization problem calculates the lowest or highest possible value of the objective function without violating any of the constraints. This can be explained by a simple example given below:

Find $x = (x_1, x_2, x_3, \ldots, x_n)$ such that,

it maximizes/minimizes the value of cost function f(x).

Subject to, inequality constraints $g_i(x) \leq 0$, i=1, 2, …

equality constraints $h_j(x) = 0$, j=1, 2, …

For topology optimization, this optimization formulation is as follows:

Objective function: When designing a component, our intentions are to increase the stiffness of the part for the given loading conditions. Hence, for topology optimization, our objective is to maximize the stiffness of the part or to minimize its compliance subject to the loading conditions.

Constraints: The main constraint for this formulation is to keep the maximum von Mises stress levels below the yield limit of the material used to avoid failure of the part. Other constraint is the volume fraction of the material to be removed or kept. This controls the amount of material to be removed from the component.

Design variables: The element density value of each element in the mesh of the design volume.

Optimization process: Instead of actually changing the shape of the part, it selects the mesh of the design volume and assigns some element density value to every element. In the first iteration, all the elements in the design volume are assigned the value given by volume fraction constraint (i.e. if the volume fraction is set at an upper bound of 0.3, it assigns all the elements in design volume an element density value of 0.3). Then the resulting stress is calculated. As per this stress distribution, it assigns a new element density value to all the elements. It is increased for the elements having stress value more than the average and decreased for the elements with stress value lower than the average. This new model is again analyzed for stress and used for next iteration. The change in maximum stress is monitored and used as a converging criterion.

Hence, the result that we get after the convergence is the element density plot of the elements ranging from a value of 0 to 1. We can select appropriate shape by selecting the threshold value (i.e. the upper limit of the element densities of the elements to be retained). It should be noted that this value is not equal to the volume of material removed.

The mathematical formulation of this process out of the scope of this study and can be found in the pioneering paper by Martin Philip Bendsoe and Noboru Kikuchi (Bendsoe and Kikuchi 1988).

5.2 Model setup in Optistruct:

Continuing from the model set up for static analysis in Hypermesh, the details of which are mentioned previously, we will now add optimization problem data.

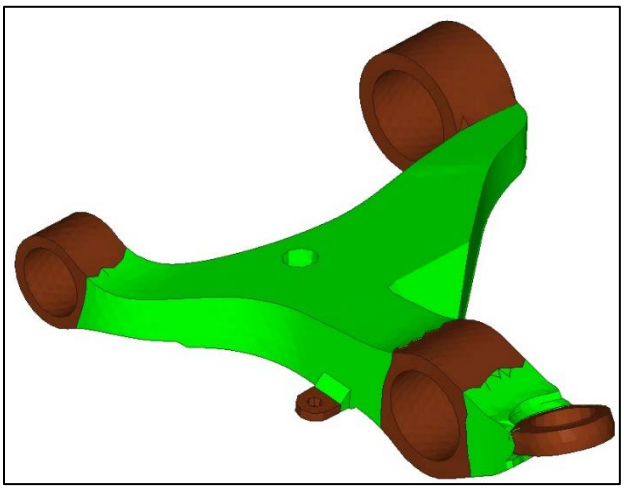

Figure 24. Design and non-design volumes of control arm

In the same way as the differential case, the control arm is divided into design and non-design volumes (as shown in Figure 24) as per the assembly requirements and stored in separate 'components' in Hypermesh. Non-design volumes (highlighted in brown color) includes areas for assembly. Design volumes (highlighted in green) can be modified to during optimization. Separate mesh is created for those two volumes.

Initially, the optimization responses that are either objective or constraints are added. This includes 'volume frac' which is used to define the volume fraction of the material to be removed and 'weighted comp' which is used to define the compliance of the part for given loading condition. Then the optimization constraints are set using the previous 'volume frac' response with an upper bound of 0.3 and an upper limit on the maximum von Mises stress of the component equal to yield of the material (490 MPa).

The objective function is created to minimize the value of the 'weighted comp' response.

5.3 Results:

The results of the optimization function in the form of the plot of the element density are as shown below in Figure 25, Figure 26, Figure 27 and Figure 28:

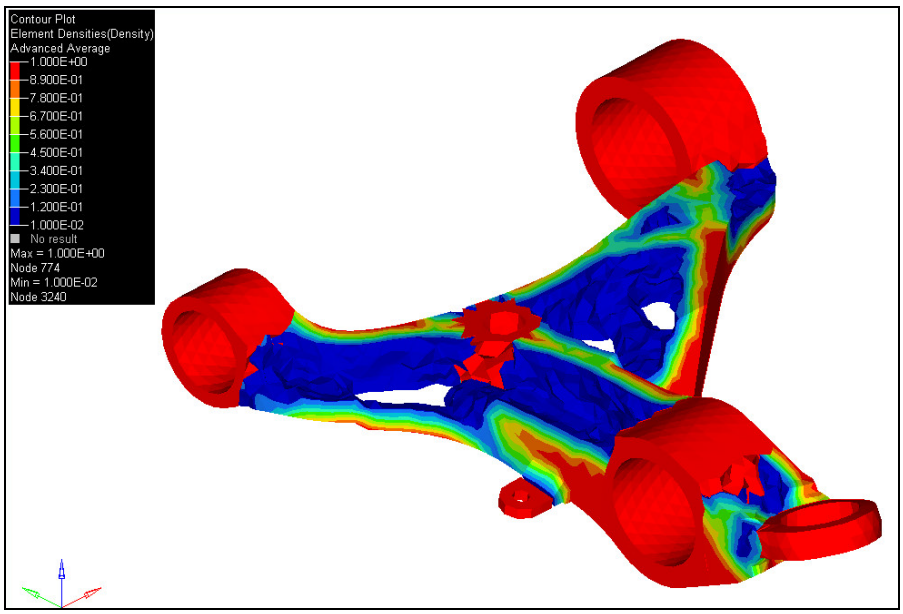

Figure 25. Optimization result considering static loading with threshold value = 0.1

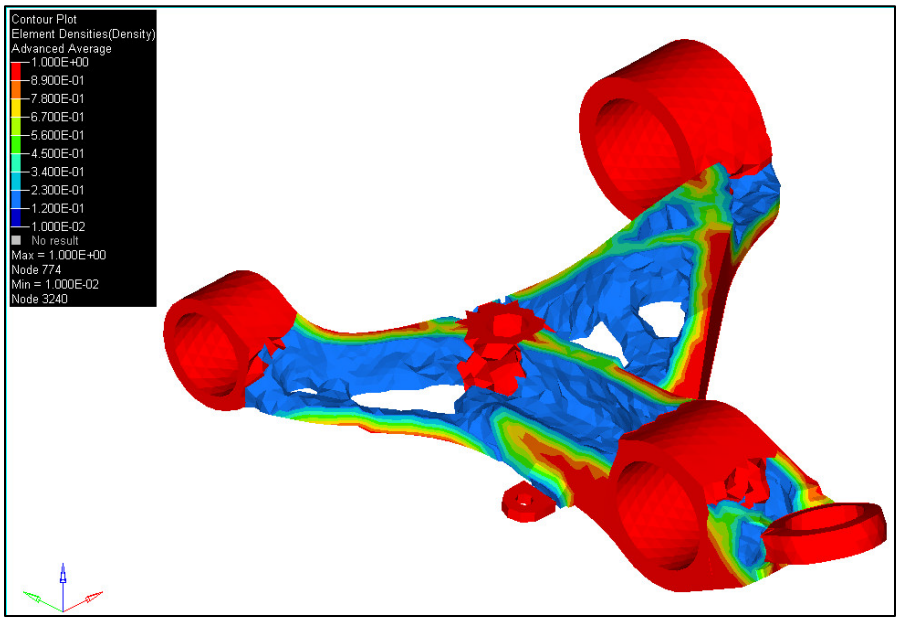

Figure 26. Optimization result considering static loading with threshold value = 0.2

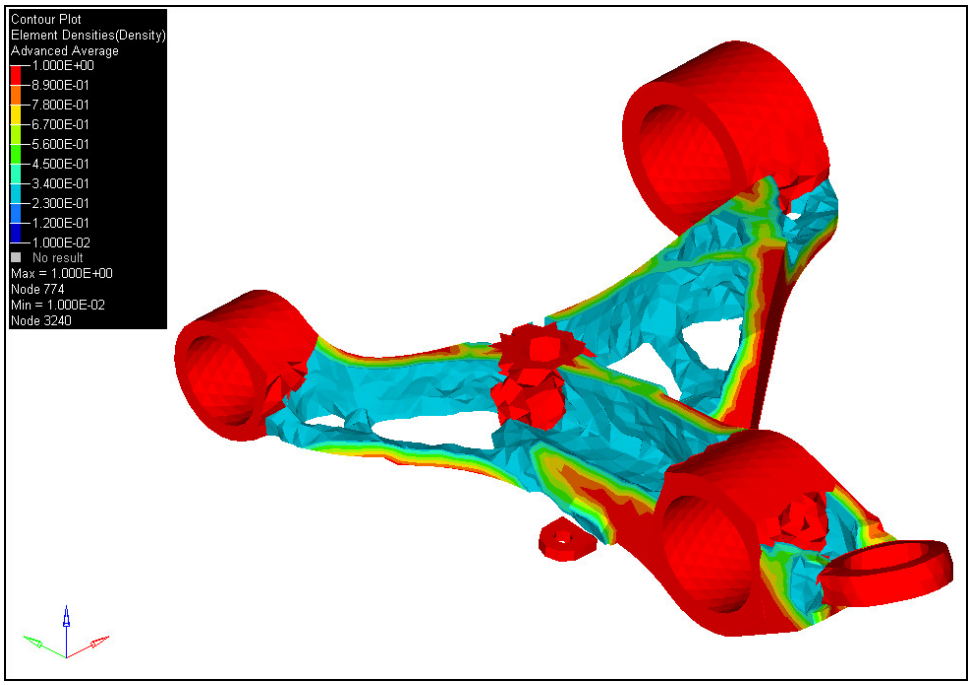

Figure 27. Optimization result considering static loading with threshold value = 0.3

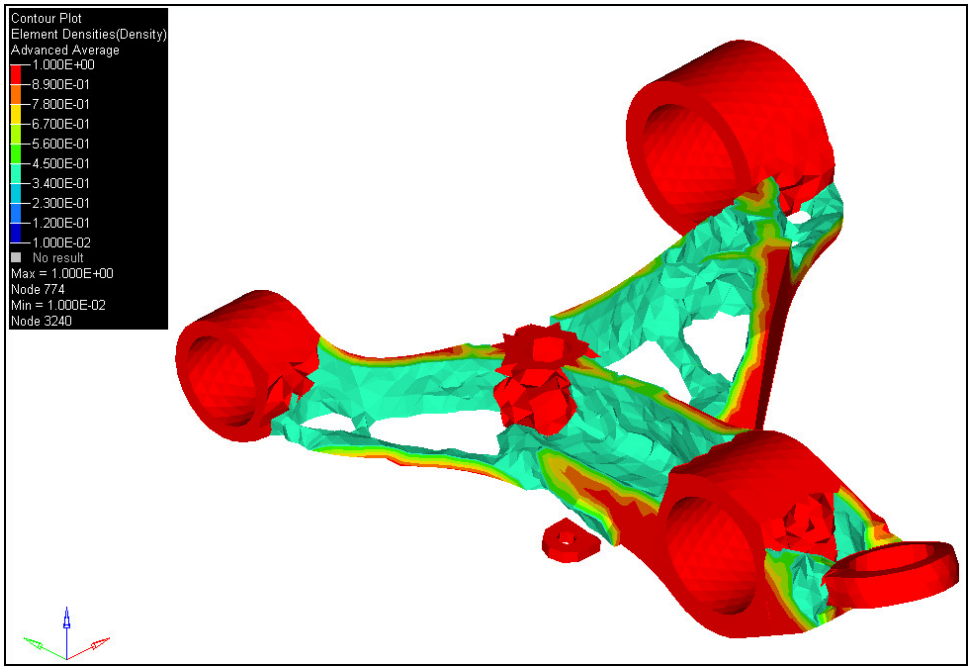

Figure 28. Optimization result considering static loading with threshold value = 0.4

6 Topology optimization for fatigue loading:

6.1 Fatigue theory:

In case of fatigue loading, we need to consider additional criteria in addition to the one mentioned above for static loading. The life of the component due to fatigue load is one such criterion and is calculated by following method:

Using the S-N curve, we can find the fatigue limit cycles for a given stress value by using the relationship:

$$\frac{N}{N_D} = [\frac{\sigma}{\sigma_D}]^k$$

Where N_D = fatigue limit cycles, σ_D= endurance limit and k = the slope of the S-N curve.

Now the damage can be calculated as,

$$D_i = \frac{n_i}{N_i}$$

For given stress amplitude i. Where n is the given number of cycles for the component and N is the fatigue limit cycle at the same stress amplitude.

Hence, we need to consider the damage of the component (or its fatigue life) while designing it for the given loading condition.

Fatigue constraint in optimization model:

In this case, we will consider part life as a criterion for design. According to the function of the part we can decide the number of cycles for which the part should perform without failing, which is the service life of the component.

Hence, for the previous optimization formulation, need to add this fatigue life constraint, which can be stated as follows:

$n_i \geq N_i$, for i=1 to total number of finite elements in the model

Where, n_i is the lowest value of life at any element in the model and Ni is the service life of the component.

In our case, the service life for a control arm is taken to be 10e8. Hence, the minimum value of the life of the optimized model must be greater than or equal to 10e8.

6.2 Model setup in Optistruct:

In addition to the previous setup for optimization of control arm with static loading, we need to add a separate response function of fatigue life using the fatigue load case that we had previously created. This response is then used to create a constrain restricting the value of fatigue life to a lower limit of 10e8 cycles. This value was selected by approximating the service life of the control arm.

6.3 Results:

The results of the optimization function in the form of the plot of the element density are as shown below in Figure 29, Figure 30, Figure 31 and Figure 32:

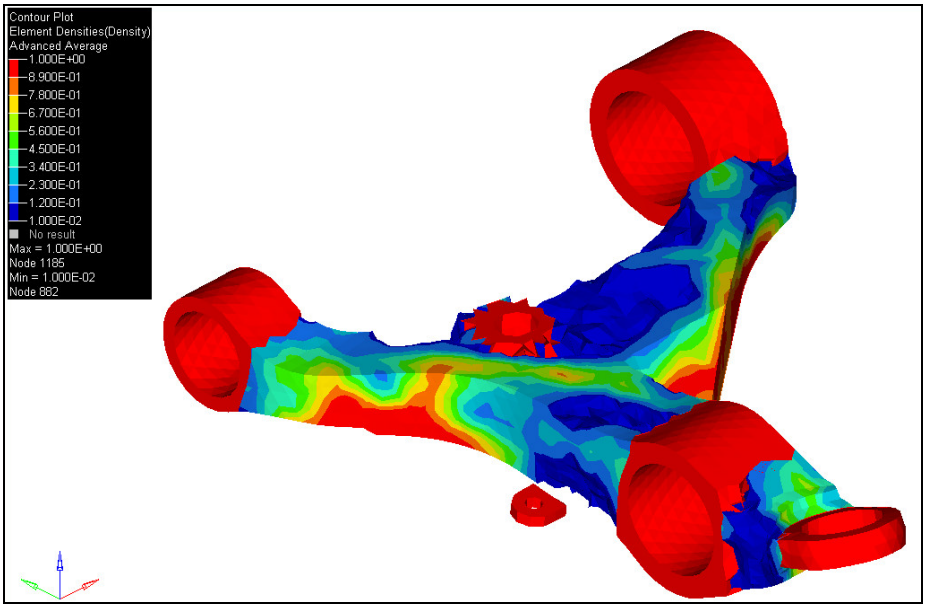

Figure 29. Optimization result considering fatigue loading with threshold value = 0.1

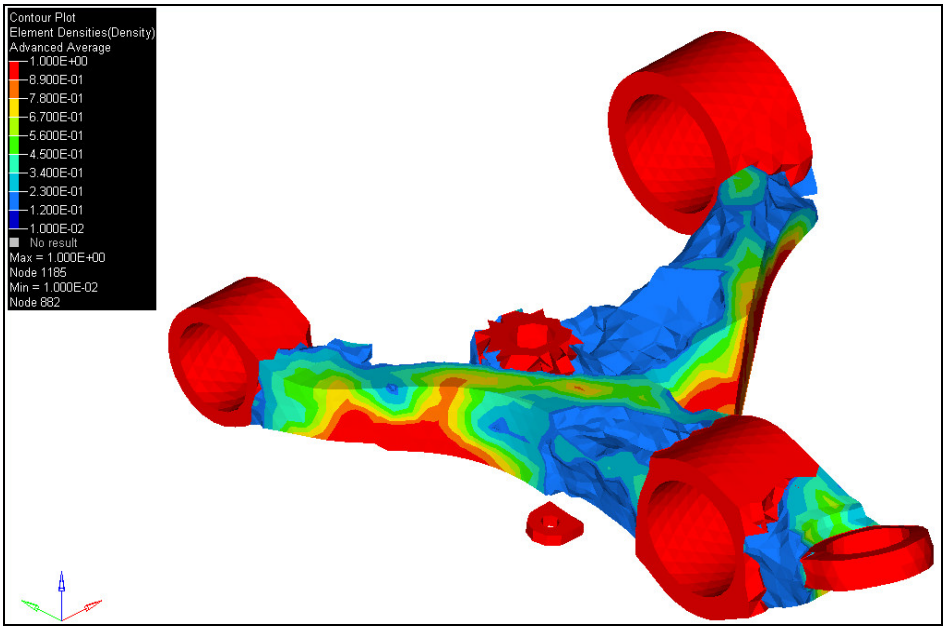

Figure 30. Optimization result considering fatigue loading with threshold value = 0.2

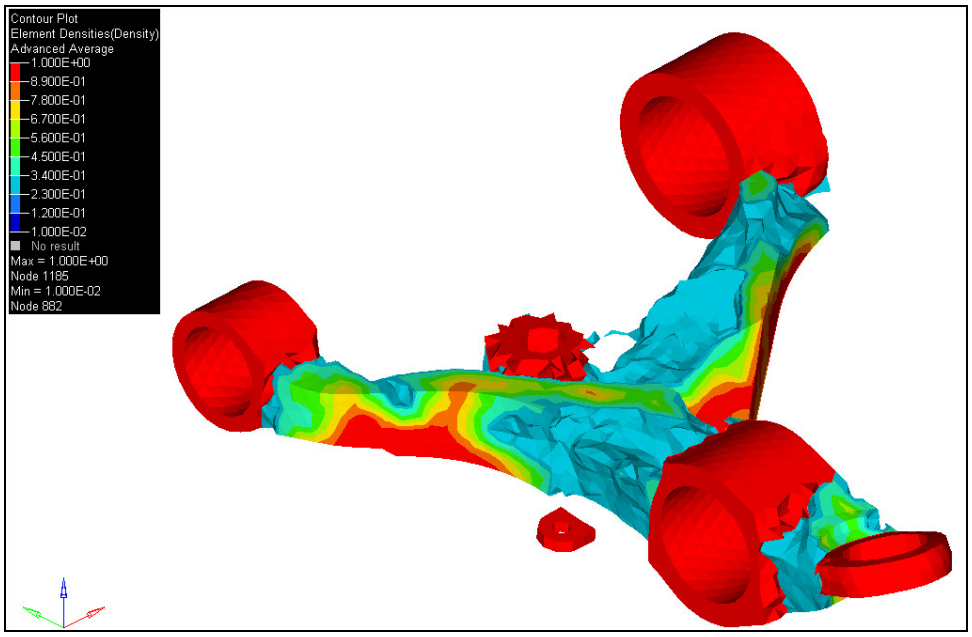

Figure 31. Optimization result considering fatigue loading with threshold value = 0.3

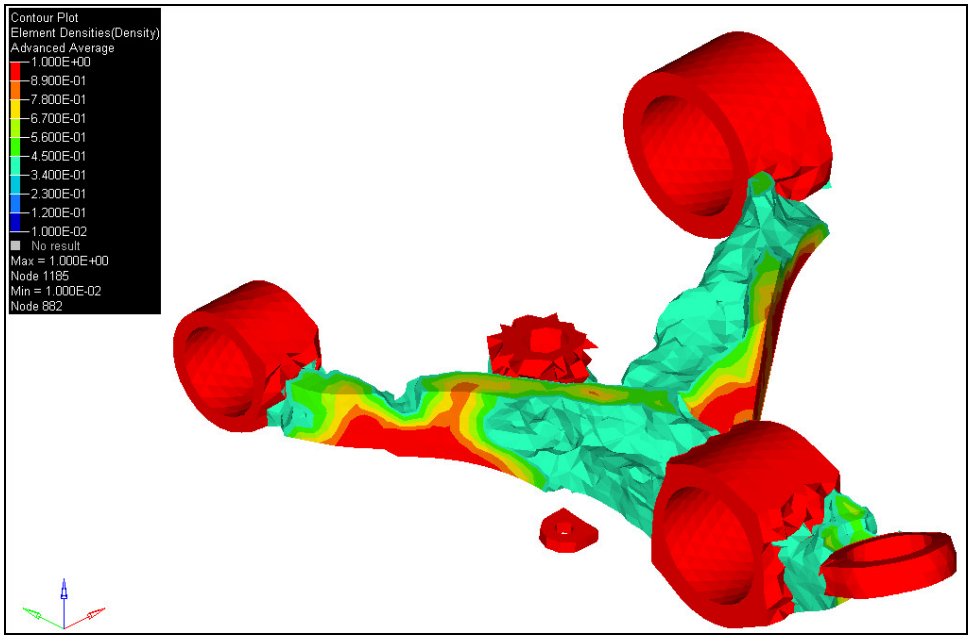

Figure 32. Optimization result considering fatigue loading with threshold value = 0.4

7 Comparison of the static and fatigue optimization results

The results obtained from static and fatigue distribution showed different element density distributions. Hence, in order to check the better design, their behavior under fatigue loading was tested. For this analysis, the threshold for each result was set in such a way that the resulting parts had same masses.

The results were selected using OSSmooth function available in Optistruct. The details of the result are given below in Figure 33, Figure 34 and Figure 35 in the form of plot of the component life and Table 6:

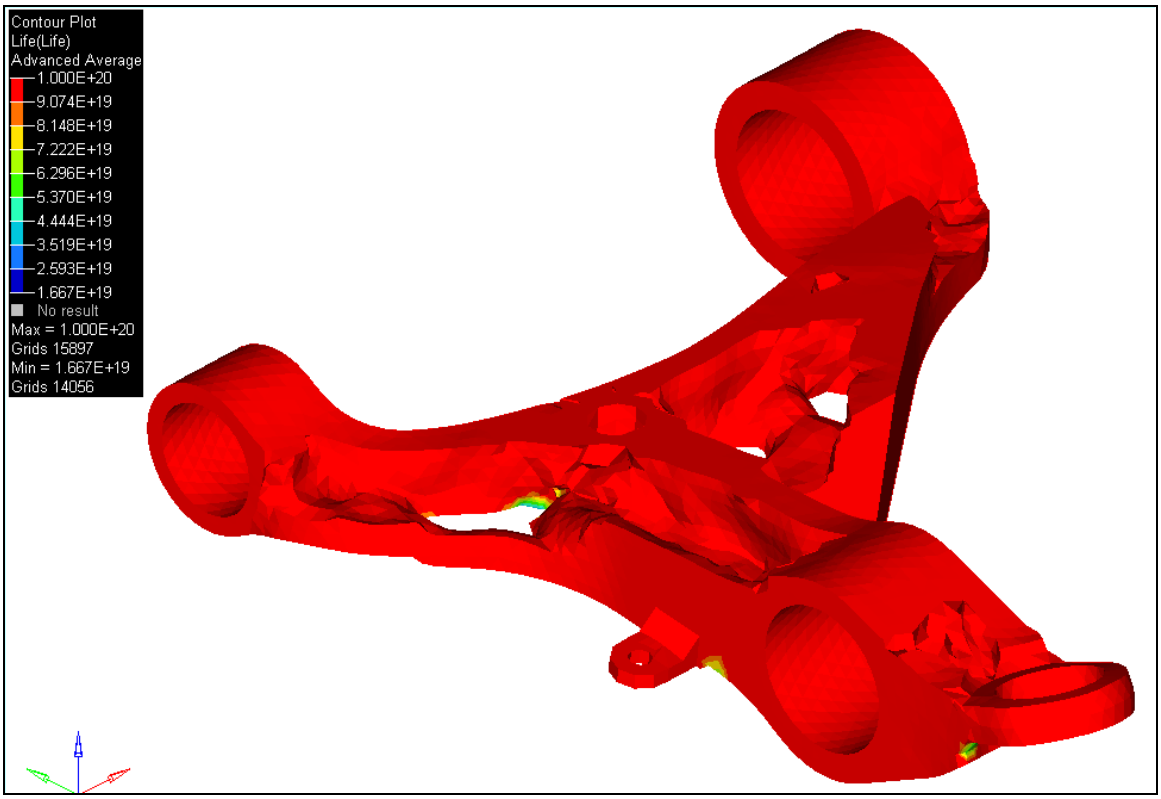

Figure 33. Life distribution for static optimization result in fatigue loading condition

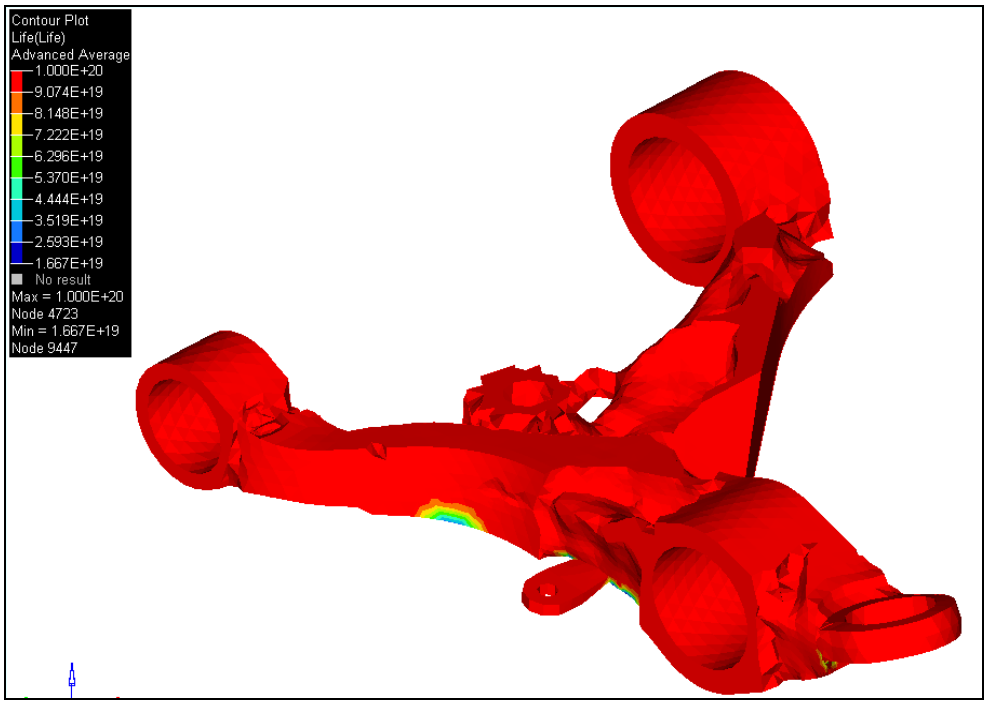

Figure 34. Life distribution for fatigue optimization result in fatigue loading condition

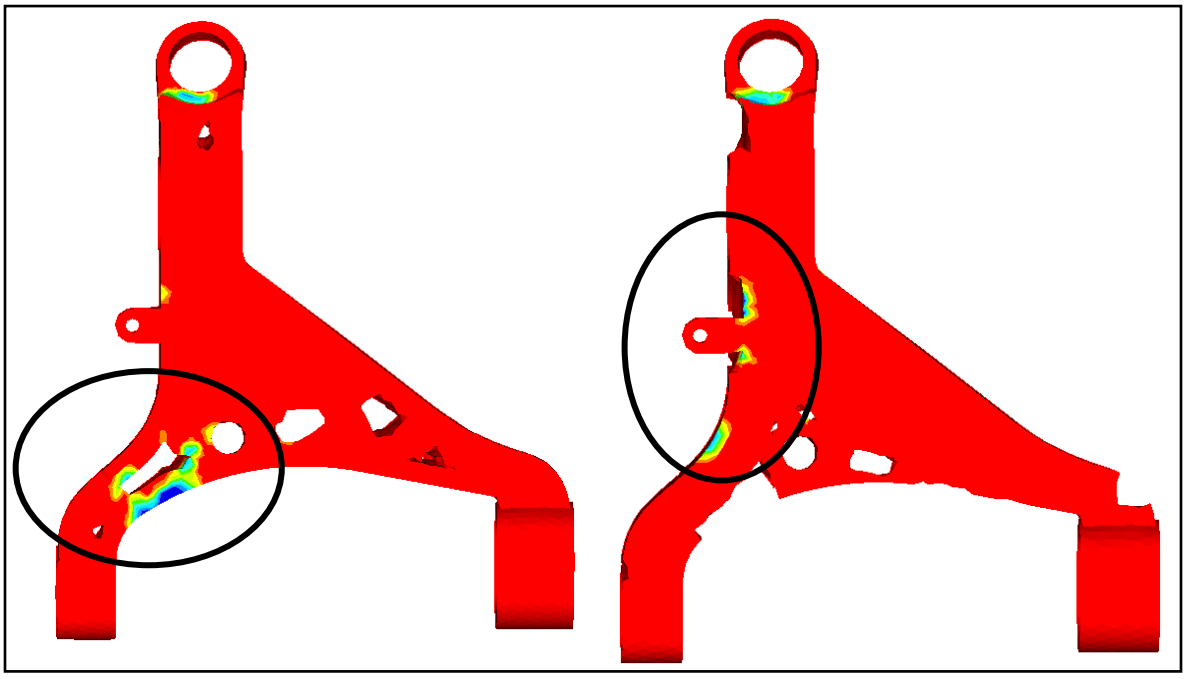

Figure 35. Comparison of life distribution for optimization results for static and fatigue loadings

Table 6. Comparison between static and fatigue optimization results under fatigue loading

Parameter	Static optimization result	Fatigue optimization result
Threshold value of model used for comparison	0.06	0.2
Volume	2.229e3	2.299e3
Lowest life	1.667e19	1.667e19

The threshold value is selected such that same amount of material is retained in both the cases. The element density assigned to the elements is much higher in the second case, which is why we had to set a higher threshold value for same volume in the second case.

The results show that the life distribution for the elements is different in both the cases. The part designed for fatigue loading shows more uniform material distribution with less cavities compared to the other one. The part designed considering static loading has all the highlighted area with lower life values concentrated near the left arm which may be disadvantageous during fatigue loading.

8 Conclusion:

1. The process of manual optimization for static loading is very time consuming (as re-meshing of the model is required for each iteration), biased (as per the stress interpretation of the person designing the component) and may not lead to best possible solution. Hence, the automatic topology optimization tools must be used for initial design guess, but only if the convergence can be met and the results are feasible.
2. Topology optimization considering fatigue loading instead of same static loading gives better solution which may perform better for the fatigue loading tests.
3. The process followed in this study can be applied to any other casting component used in automobiles with minor modifications to achieve weight reduction.

9 References:

"Hyperworks help manual, 14.0."

(2015). "Market Trends." greenercars.org. from http://www.greenercars.org/greenest-meanest/market-trends.

(2015). "Market Trends." Greener Cars. American Council for an Energy-Efficient Economy.

(2016). "Altair website." from ftp://ftp.altair.com.cn/priv/support/hw11.0/...0_pdf.../OptiStruct_11.0_Tutorials.pdf.

Bendsoe, M. P. and N. Kikuchi (1988). "Generating Optimal Topologies in Structural Design Using a Homogenization Method." Computer Methods in Applied Mechanics and Engineering **71**(2): 197-224.

Cole, G. S. and A. M. Sherman (1995). "Lightweight Materials for Automotive Applications." Materials Characterization **35**(1): 3-9.

Deshpande, P. S. (2016). Design optimization process of differential case. Michigan Technological University.

Kelkar, A., et al. (2001). "Automobile bodies: Can aluminum be an economical alternative to steel?" Jom-Journal of the Minerals Metals & Materials Society **53**(8): 28-32.

Reinl, A. D. (2016). "Effects of Cooling Rate and Alloy Chemistry on the Microstructure and Mechanical Properties of Thin Wall Ductile Iron."

Song, B. C., et al. (2009). "Structural optimization of an upper control arm, considering the strength." Proceedings of the Institution of Mechanical Engineers Part D-Journal of Automobile Engineering **223**(D6): 727-735.

Uwe Schramm, M. Z. (2006). "Recent Developments in the Commercial Implementation of Topology Optimization." IUTAM Symposium on Topological Design Optimization of Structures, Machines and Materials: 239-248.

Witik, R. A., et al. (2011). "Assessing the life cycle costs and environmental performance of lightweight materials in automobile applications." Composites Part a-Applied Science and Manufacturing **42**(11): 1694-1709.

Wu, D., Richard Roth, and Randolph Kirchain (2016). Energy Saving and Greenhouse Gas Emissions, Massachusettes Institute of Technology.

Appendix A

Material addition to reduce stresses (Initial model is highlighted in blue and the updated one after material addition is highlighted in green)

1.

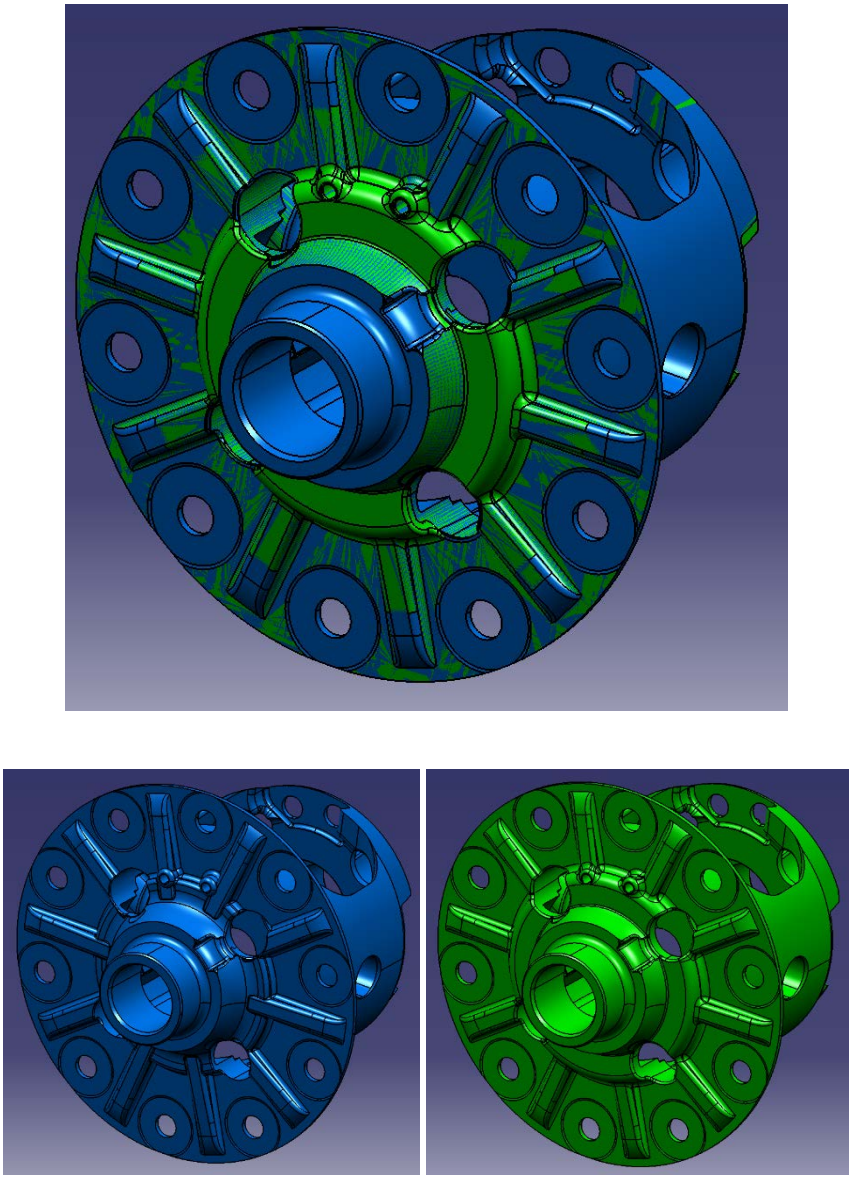

Figure 36. Material addition details 1

2.

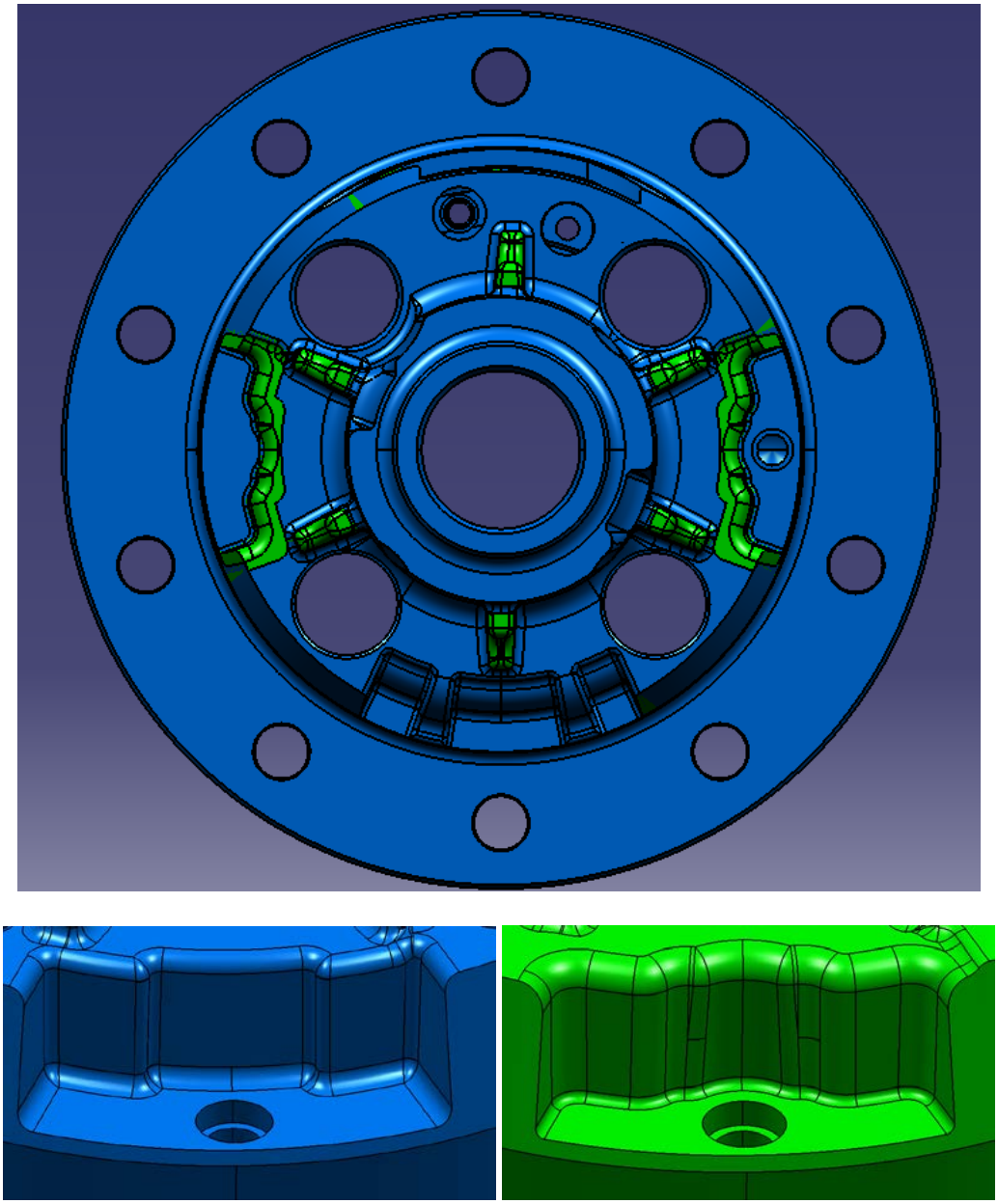

Figure 37. Material addition details 2

3.

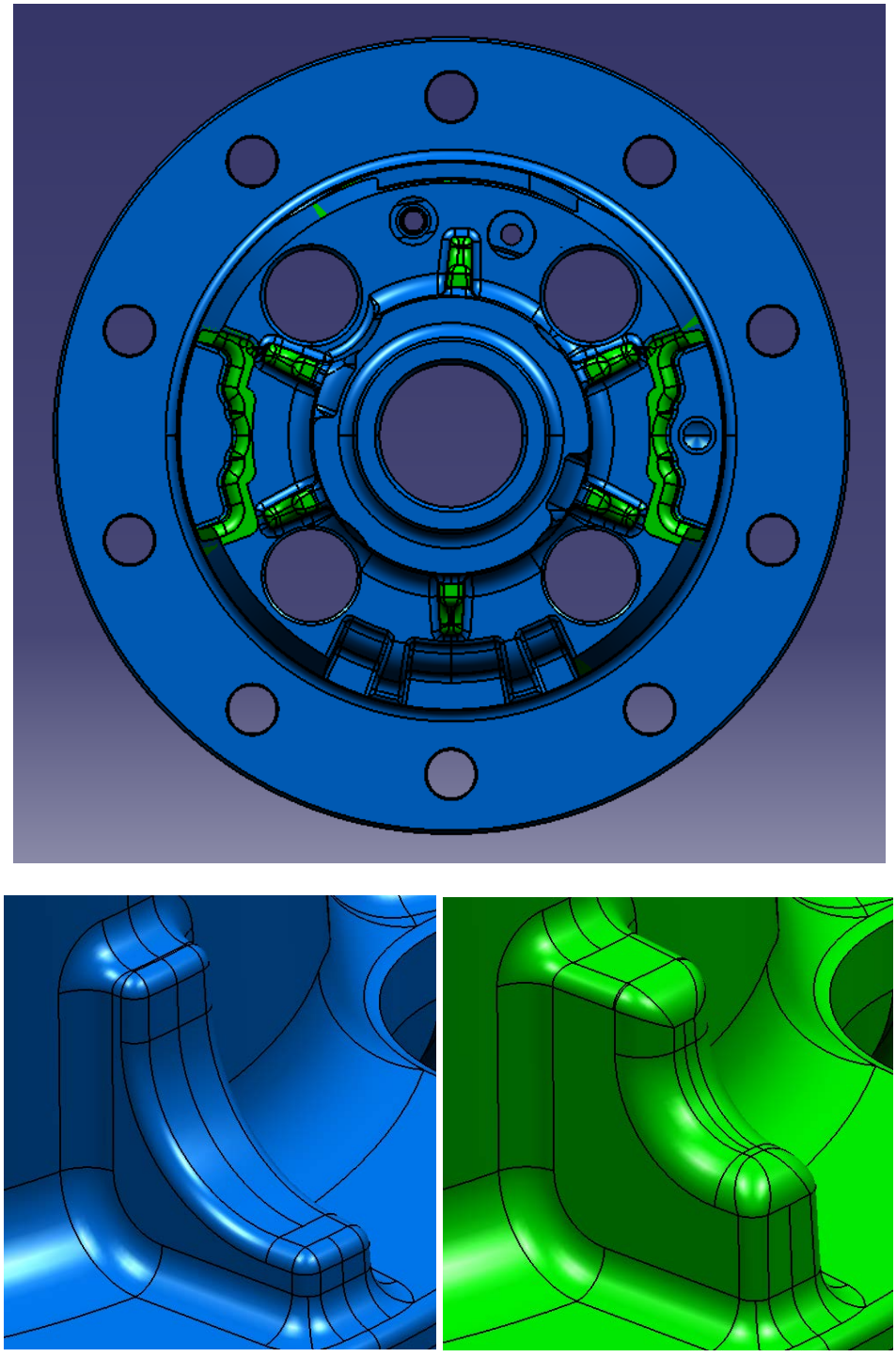

Figure 38. Material addition details 3

4.

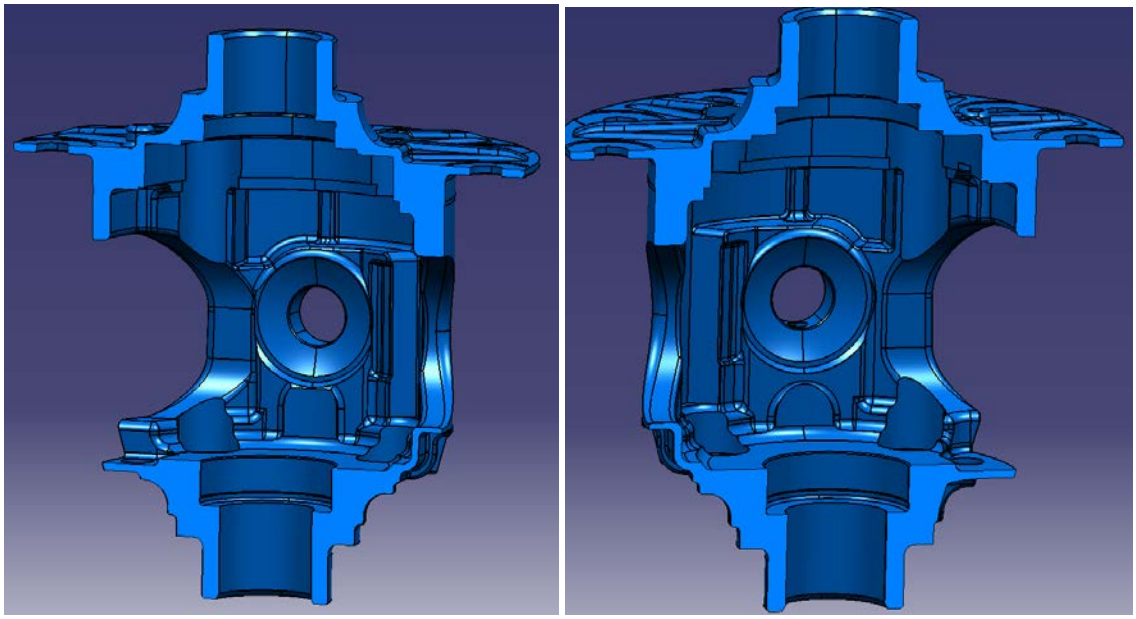

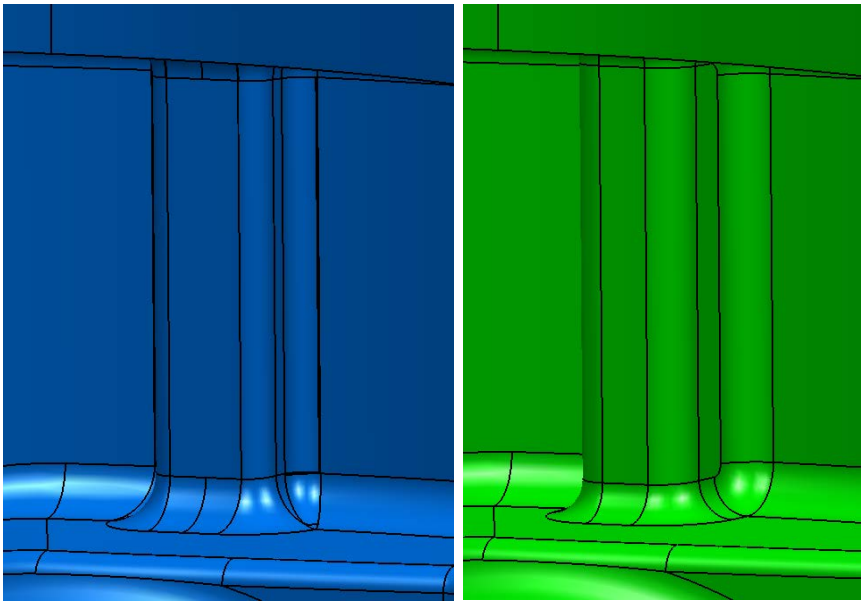

Figure 39. Material addition details 4

5.

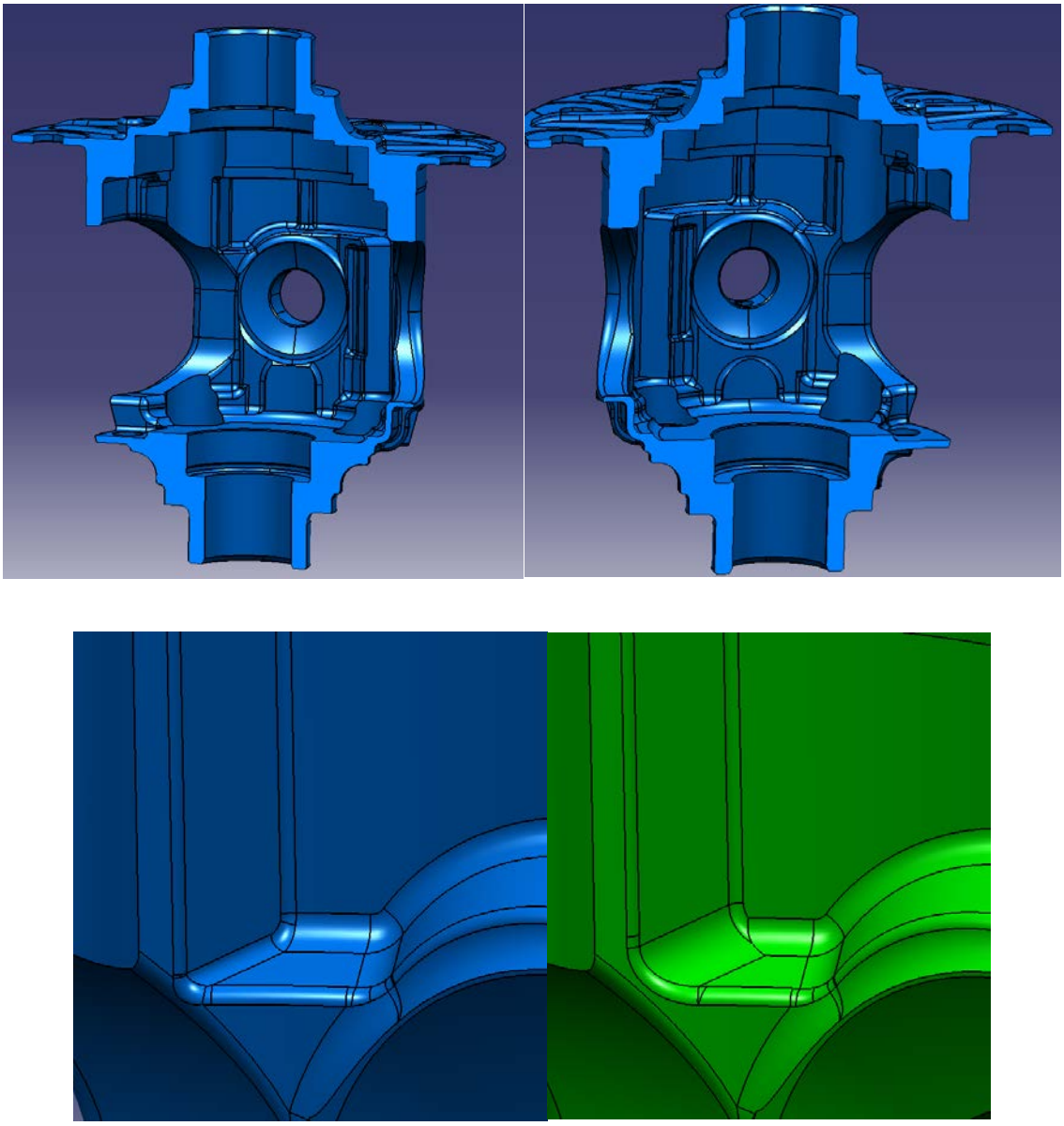

Figure 40. Material addition details 5